MINISTRY OF EDUCATION
National University of Science and Technology
POLITEHNICA Bucharest

Doctoral School of
Industrial Engineering and Robotics

Adrian F. FLOREA

The summary of the PhD THESIS

RESEARCH ON WELDING HIGH-STRENGTH STEELS

Scientific coordinator,
Prof. univ.dr.ing. Corneliu RONTESCU
(POLITEHNICA Bucharest)

- 2025 -

Contents

Keywords:

Welding, High-Strength Steels (HSS), S890QL, Weldability, Robotic Cell, Gas Metal Arc Welding (GMAW), Cooling Time ($t_{8/5}$), Preheating Temperature, Microhardness, Microscopic Analysis, Mechanical Properties, Thermal Field, Experimental Validation, Computational Fluid Dynamics (CFD), Finite Element Modeling (FEM).

Chapter 1. Current state of high-strength steel applications in welded constructions

1.1 Introduction

High-strength steels have been employed in various industrial sectors since the 1950s, but their characteristics have evolved significantly over time. In the 1960s, the maximum yield strength of weldable high-strength steels was approximately 400–500 MPa, whereas modern high-strength steels (HSS) can now achieve yield strengths exceeding 1300 MPa. In recent years, the demand for modern high-strength steels has increased due to their significant advantages in terms of weight [1], these steels offer both high strength and low weight, enabling the reduction of structural thicknesses and enhancing energy efficiency in their applications. High-strength steels are used in a wide range of industrial fields and applications, including the automotive industry, shipbuilding, hydroelectric and nuclear power plants, forestry and agricultural applications, oil extraction platforms, pipelines, trucks, logging cranes, and other lifting equipment. Examples of high-strength steels applications in the automotive industry are shown in Figure 1.1.

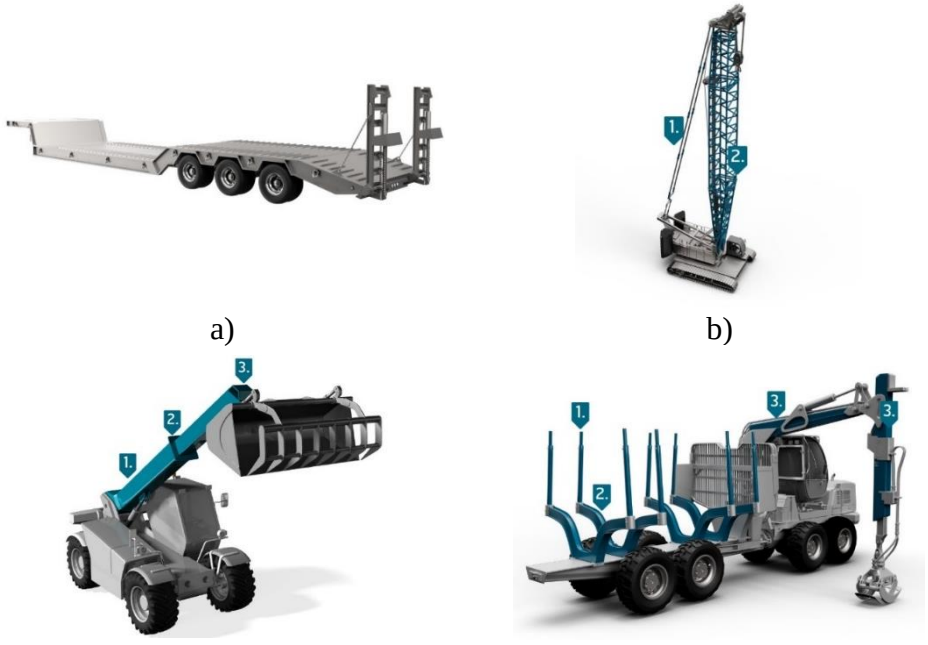

a) b) c) d)

Fig.1.1 Examples of high-strength steels applications in the automotive industry: a – automotive platforms, b – lifting systems, c – loading/transport systems, d - forestry transport equipment, 1,2,3 – components made from high-strength steels. [2]

The predominant method for joining steel structures is welding, and welding high-strength steels has been the focus of extensive research in recent years. Ensuring high-quality welded joints requires a thorough understanding of the factors influencing the weldability of these steels, including their manufacturing method and chemical composition. The relationship between welding parameters such as heat input (defined by welding current, arc voltage, and welding speed), cooling time, and preheating temperature is a classic issue in identifying optimal values. These parameters significantly influence the welding process, and changing of one parameter can have substantial effects on both the quality of the welded joint and the properties of the materials used.

Welding high-strength steels requires strict control of welding parameters, which are influenced by the steel's manufacturing process and chemical composition. Although research on welding these steels are still ongoing, there is not yet sufficient data to provide on the choice of optimal welding parameters for different types of high-strength steels and welding processes. This raises the question of how welding

parameters for various steel types and processes can be standardized to predict the properties of the welded joints executed.

Despite technical recommendations from various high-strength steels manufacturers, such as ESAB (Washington DC, USA), SSAB (Stockholm, Sweden), Dillinger (Stuttgart, Germany), and ThyssenKrupp (Essen, Germany) [2, 14, 15, 16], there is no unified scientific methodology applicable to all welding processes. This highlights the need for a deeper understanding of the welding characteristics of high-strength steels and the development of practices that ensure superior quality welded joints.

1.2 Classification of high-strength steels

The continuous development of manufacturing processes has enabled the production of steels not only with higher strength but also with improved toughness, better weldability, enhanced cold workability, and increased corrosion resistance. These advancements have made high-strength steels an attractive material for structural applications, particularly when considering manufacturing costs, energy savings, material costs, and the reduction of CO2 emissions over the entire lifecycle of weight-critical welded construction projects [17].

The evolution of high-strength steels development is illustrated in Figure 1.2.

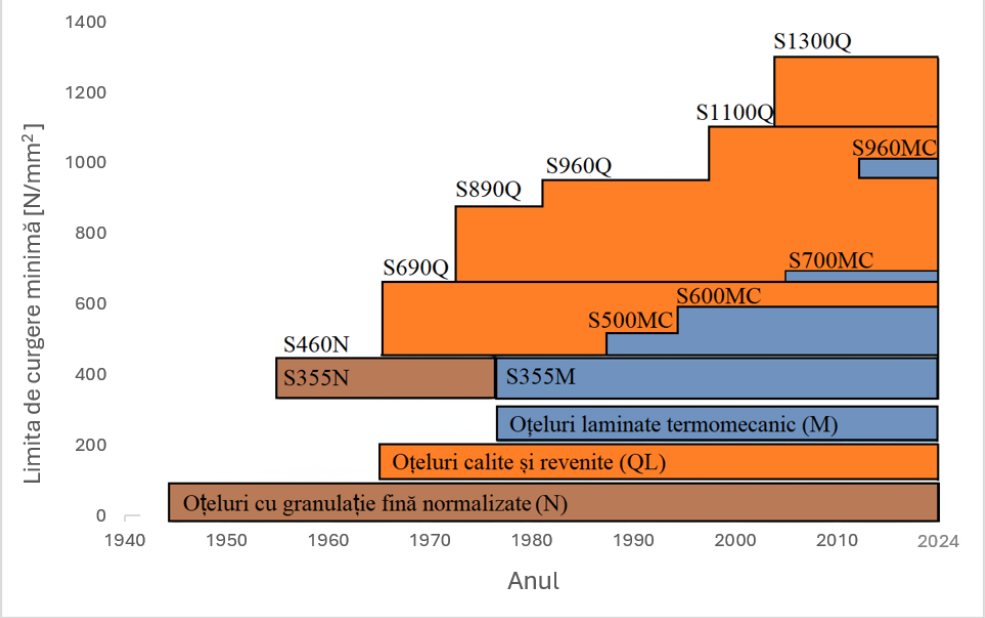

Fig.1.2 The evolution of high-strength steels: - Normalized Steels; Thermomechanically Rolled Steels; - Quenched and tempered steels. [10]

The main heat treatments applied for the development of high-strength steels are: normalization (N), thermomechanical controlled rolling (M), and quenching and tempering (Q) [13].
Some normalized fine-grained steels exhibit moderate strength of up to 460 N/mm², while certain thermomechanically rolled steels can have a yield strength of up to 690 N/mm², whereas quenched and tempered steels can reach very high fracture strength values of up to 1300 N/mm² [22].

1.3 Particularities of High-Strength Steels

The main characteristics of high-strength steels are their mechanical strength and high level of toughness. It is important to emphasize that, depending on the specific conditions of use, the effects of mechanical stresses, temperature, and time on these properties must be carefully evaluated. Additionally, a thorough understanding of the behavior of these steels during welding is of particular importance.

1.4 Conclusions regarding the use of high-strength steels in welded constructions

- The continuous development of industrial manufacturing processes, with increasingly higher demands regarding the stresses during manufacturing, has led to the necessity of creating materials that ensure high mechanical properties while maintaining high fracture energy at low temperatures.
- The development of high-strength steels (HSS) began in the mid-20th century, with the emergence of normalized steels having a fracture strength value of 400–500 MPa (S355N/NL, S460NL/ML), reaching today values of 1400 MPa for ultra-high strength steels (S1300Q – see § Figure 1.2), or 1700–2000 MPa for advanced high-strength steels (MS 1250/1500) [37].
- High-strength steels are used for their high mechanical properties, corrosion resistance, and fracture energy at low temperatures, thus ensuring significant weight reduction of the structure and enabling their use in different environmental conditions.
- High-strength steels are used in various industrial fields. In the mid-20th century, normalized steels began to be used for the fabrication and repair of storage and transportation tanks and containers through welding. With the development of this category of steels, their applicability has expanded into different industrial fields: automotive (structural strength), railway transport (tanks for transport, infrastructure), offshore drilling platforms, shipbuilding, energy (wind turbines, transmission towers, and other energy-related structures), construction and infrastructure (buildings, bridges), and heavy equipment manufacturing (lifting equipment, excavators, bulldozers, and other excavation machinery).

Chapter 2. Current status regarding the welding of high-strength steels

2.1 Welding behavior of high-strength steels

High-strength steels, subjected to heat treatments to improve their mechanical properties, exhibit good weldability and can be welded by most available processes. However, certain technological issues may arise during welding, among which the following stand out:

- *Cold cracking*, caused by structural transformations (formation of hard structures such as bainite or martensite) in combination with the presence of diffusible hydrogen in the material, as well as stresses generated during the welding processes.
- *Degradation of toughness properties*, manifested by a reduction in fracture energy under dynamic loading and an increase in the ductile-to-brittle transition temperature, factors strongly influenced by the steel's microstructure, especially by the type and distribution of precipitates formed during the cooling process.

Weldability is closely related to the material's yield strength. During the welding process, particular attention must be given to the steel's susceptibility to cold cracking, a phenomenon influenced by internal stresses that arise during welding, the presence of diffusible hydrogen (from the base material, filler material, surrounding environment, etc.), and the hard, brittle structure. Regardless of the type of steel used, strict control of the heat input during welding is essential. In particular, the preheating temperature must be properly managed to minimize cracking risks and ensure the integrity of the welded joint [25].

2.1.1 Weldability of normalized steels

Fine-grained normalized steels have good weldability if the recommendations from the EN 1011-2:2002/A1:2004 and SEW 088:2017 standards [38..40] are followed. Fine-grained steels are deoxidized steels, characterized by the presence of nitrides and carbides in the crystalline structure, formed at high temperatures. These fine precipitates prevent grain growth in the austenitic phase and result in the formation of a fine grain structure.

For these steels, under certain conditions, preheating to a specific temperature is necessary to prevent cold cracking [41]. An important parameter in this process is the weld cooling rate, indicated by the $t_{8/5}$ value, which represents the time required for the weld to cool from 800°C to 500°C. Fine-grained normalized steels exhibit good welding behavior and can be welded by practically any welding process, but some issues may arise, such as cold cracking or deterioration of toughness characteristics due to a decrease in impact energy and an increase in the ductile-to-brittle transition temperature. These phenomena are mainly influenced by the metallographic structure and the distribution of precipitates.

2.1.2 Weldability of thermomechanically rolled steels

Thermomechanically treated steels are known for their weldability due to their low carbon content (carbon equivalent). These steels offer superior welding performance compared to normalized steels, with a significant reduction in elements that contribute to hardening.

This reduction in carbon equivalent makes thermomechanically rolled (TM) steels and those with accelerated cooling (AC) less prone to cold cracking compared to conventional steels, and the preheating temperatures required for welding are lower. The welding conditions for these steels are similar to those for normalized steels.

Welding of thermomechanically treated steels can be carried out with most welding methods. The choice of filler material is important to ensure the quality of the welded joints. Typically, the strength of the filler material is similar to that of the base material, although in some cases, filler materials with lower strength are preferred. In these cases, the filler material should have a chemical composition with a higher concentration of hardening elements and, as a result, greater sensitivity to cold cracking than the base material. [25, 48, 49, 50].

2.1.3 Weldability of quenched and tempered steels

The weldability of quenched and tempered steels is weaker compared to other types of steels. Depending on their composition, they may be weldable under specific conditions or even unweldable. Weldability is influenced by the material's yield strength, and attention must be focused on its sensitivity to cold cracking. In all cases, it is necessary to control the heat input into the base material during welding, as well as adhere to preheating temperatures.

The main factor to consider when welding fine-grained steels is the evolution of the thermal field, which influences the Heat-Affected Zone (HAZ) through:

- The tendency to harden due to the formation of martensite and the increased risk of cracking.
- The recombination of diffusible hydrogen is more pronounced in fine-grained steels due to the size of the grain boundaries, creating more potential zones for hydrogen recombination.

Preheating is essential to prevent cold cracking and other defects [53]. It allows for the removal of hydrogen and reduces internal stresses. In multi-pass welding, preheating may be omitted for the first pass if an adequate temperature is maintained between passes.

2.2 Technological elements in welding high-strength steels

Weldability is determined by the metallurgical, technological, and welded construction behavior of the base material subjected to the welding process. Equivalent carbon, linear energy, preheating temperature, and cooling time significantly influence the welding process outcomes.

Residual stresses arise from the uneven distribution of heat during welding and from the behavior of materials during the heating and cooling processes. The fatigue strength of the welded joint is higher when residual stresses are reduced.

2.2.1 Equivalent Carbon

The metallurgical behavior of welding low-alloy steels, which have a particularly wide range of applications, is primarily determined by their chemical composition. This behavior is commonly assessed based on the equivalent carbon content (CET). Over the past 50 years, numerous formulas for calculating the equivalent carbon have been developed [62], based on the results of tests (hardness, resilience, cold cracking, metallographic, etc.) for welds made in single-pass or multi-pass conditions, under various technological conditions [63].

2.2.4 Cooling time $t_{8/5}$

A global indicator for analyzing the thermal cycle in welding is represented by $t_{8/5}$. It is observed that the cooling time is inversely related to the cooling rate, meaning that a large $t_{8/5}$ corresponds to a slow cooling rate and vice versa [69].

The cooling time from 800°C to 500°C is the most important parameter influencing the properties of the welded joint in HSS, especially the microstructure of the heat-affected zone (HAZ) [70..73]. This is influenced by the amount of heat input, preheating and interpass temperatures, steel thickness, and the shape of the weld [74..76].

The cooling time from *800°C to 500°C*, $t_{8/5}$, is determined analytically and with the help of diagrams/nomograms, depending on the type of heat conduction, whether two-dimensional or three-dimensional, occurring during the welding process[40, 54].

2.3 Fusion welding processes used for joining high-strength steels

Currently, numerous welding processes [81, 82], are available, which can be classified based on the energy source used to create the joints. In most cases, the energy used is of an electrical nature, transformed into heat through the electric arc or the Joule-Lenz effect. Additionally, thermal energy can be generated through oxy-gas flames, thermochemical reactions, electron and photon beams, ultrasound, and mechanical friction [54].

Fusion welding involves melting and joining materials, often with the addition of filler material in the welding zone to facilitate the connection. Among the welding techniques, electric arc welding is one of the most commonly used, where the energy generated by the arc melts both the surface of the parts to be joined and the filler material (such as coated electrodes, wires, or rods).

2.4 Conclusions regarding the welding of high-strength steels

- The weldability of high-strength steels is conditioned by the carbon content, as well as the alloying elements, with the equivalent carbon being a general criterion for analyzing the weldability of these types of materials.
- The main issues regarding the weldability of high-strength steels are related to the risk of cold cracking (due to the formation of hard and brittle structures, the presence of internal stresses, and diffusible hydrogen) and the loss of toughness properties, manifested by a reduction in fracture energy under dynamic loading and an increase in the ductile-to-brittle transition temperature (due to grain coarsening).
- For successful welding of high-strength steels, it is recommended to perform preheating (to prevent cold cracking) and to use stringer bead welding (to avoid grain growth).
- Most classical fusion welding processes can be used to make joints in high-strength steels, with particular attention given to processes where heat dissipation occurs rapidly (such as EBW and

LASER), as there is a risk of forming hard and brittle structures and excessively increasing the mechanical properties in the heat-affected zone (HAZ) and the welded joint.

Chapter 3. Objectives and structure of the doctoral thesis. research equipment.

3.1 Objectives of the doctoral thesis

The choice of the doctoral thesis topic starts from the practical need to reduce the size and weight of products used in various industrial sectors. The specific case analyzed in this work is the reduction of the weight of the chassis of a rail welding installation (figure 3.1.)

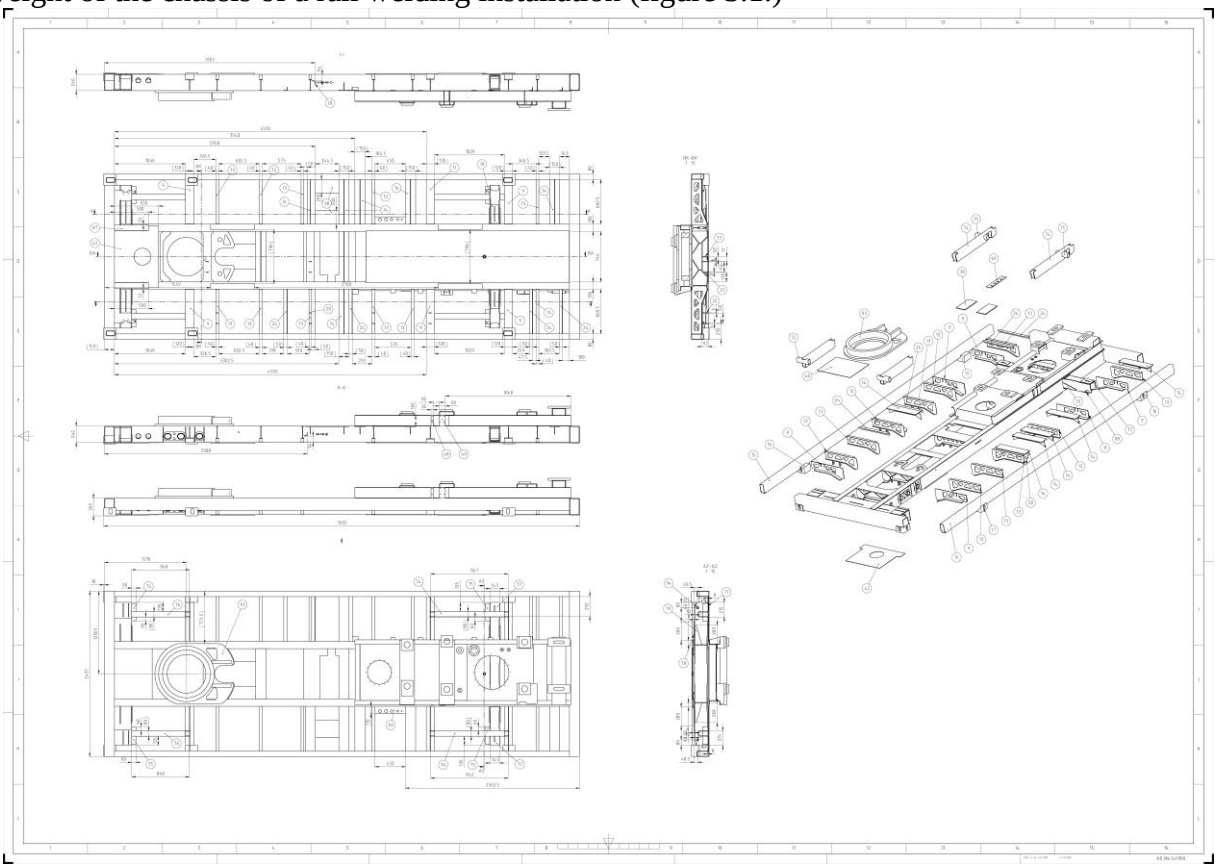

Fig. 3.1. Execution drawing of the chassis for the rail welding installation (FBW machine)

The reduction in product weight can be achieved by decreasing the thickness of the components used in the welded assembly of the chassis. Under these conditions, it is necessary for the base materials used in manufacturing the components of the assembly to exhibit superior mechanical and functional properties, compensating for the reduced thickness while maintaining strength and integrity under operational stresses.

Considering this practical necessity, it is proposed to replace the S355 ML base material, currently used in the welded construction of the chassis assembly, with a high-strength steel material.

The primary objective of the doctoral thesis is the development of welding technologies for S890QL steel in the context of its use as the base material for the manufacturing of the chassis for the rail welding installation.

Fig. 3.2. Chassis for the rail welding installation

In the doctoral thesis, based on the current state of knowledge, the theoretical research covered the following aspects:

- Understanding the main types of high-strength materials, highlighting their historical evolution and mechanical properties.
- Identifying the main weldability issues encountered when welding high-strength materials.
- Understanding the primary fusion welding processes used for high-strength materials, including their advantages, disadvantages, and specific limitations in applicability.

The experimental research focused on the following objectives:

- Developing an experimental plan for assessing the weldability of the high-strength steel S890QL.
- Creating welding technologies for S890QL material to replace the base material S355ML.
- Implementing the experimental plan and conducting experimental research on welding S890QL steel.
- Performing nondestructive testing on the welded samples made from S890QL steel.
- Conducting destructive testing on the welded samples made from S890QL steel.
- Measuring and validating the cooling time t8/5 using various experimental methods (including contact thermocouples and infrared thermography).
- Finite element modeling of the thermal field during welding and measuring the technological parameter t8/5.
- Finite element modeling of the operational behavior of the welding equipment chassis made from base materials S355ML and S890QL.

3.2 Structure of the doctoral thesis

Based on the objectives outlined in Subchapter 3.1, a general schematic for all activities undertaken within the scope of the thesis has been developed, as shown in Figure 3.3.

The general activity schematic was founded on the knowledge gained through the theoretical analysis of the main high-strength materials, their chemical composition, properties, welding behavior, and applicable welding processes. Additionally, it incorporates the practical experience accumulated in the workplace.

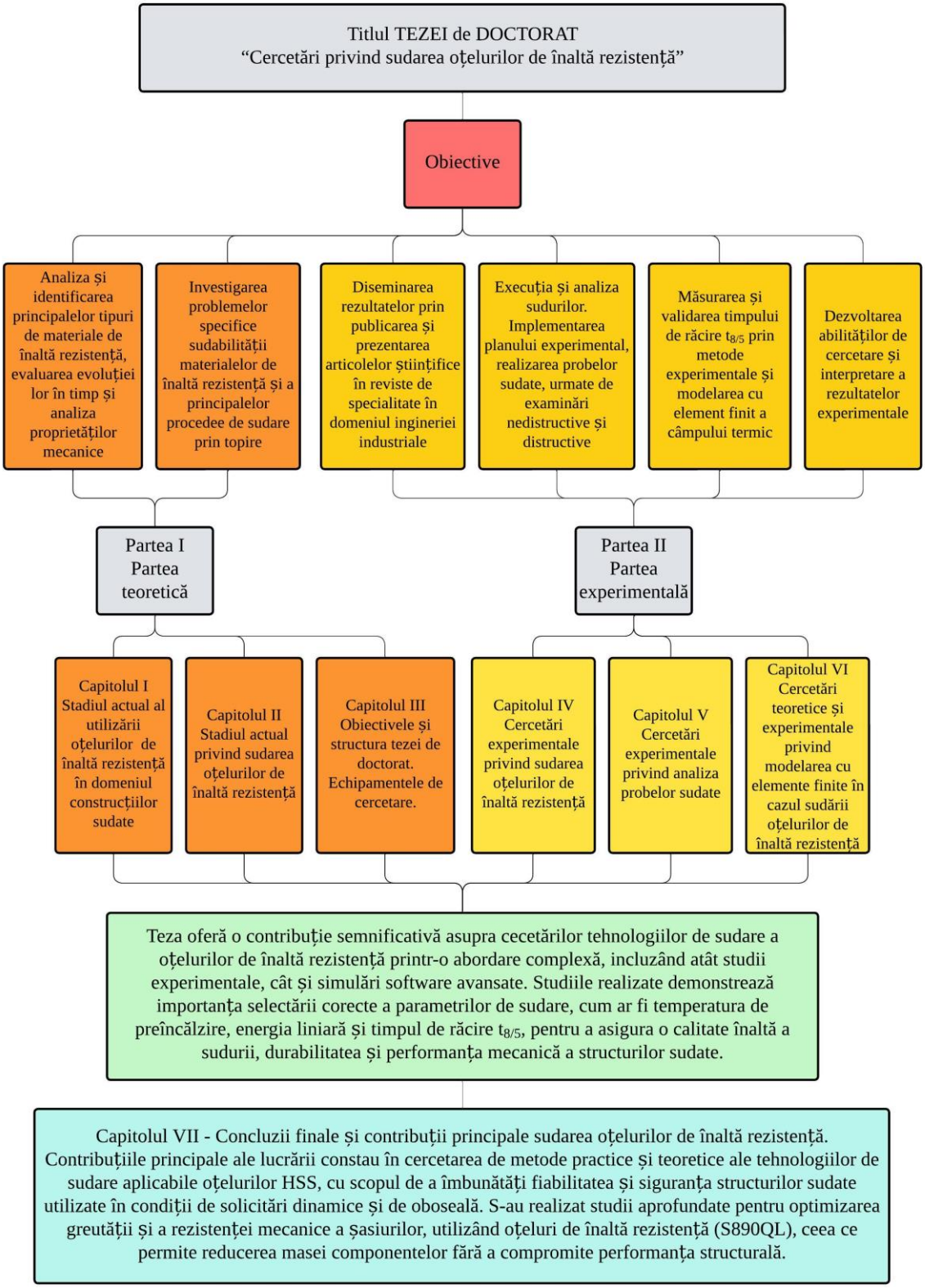

Fig. 3.3. Structure of the doctoral thesis

3.3 Research equipment used in the experimental program

Based on the knowledge gained from studying the specialized literature on the weldability of high-strength steels, as well as practical experience accumulated in the workplace, an experimental plan was developed to investigate the weldability of S890QL steel.

The experimental program involved welding 12 samples using the robotic GMAW process. After welding, the samples underwent non-destructive and destructive testing to assess their quality and identify valid welding technologies.

The experimental program, as well as the examinations and tests conducted, utilized equipment from the laboratories of the University Politehnica of Bucharest and from collaborating companies.

3.3.1 Welding equipment for S890QL steel samples

The samples were welded using the Fanuc ARCMate 100iBe robotic cell, located in the Robotic Welding Laboratory of the Department of Quality Engineering and Industrial Technologies (ICTI), within the Faculty of Industrial Engineering and Robotics (FIIR) (Figure 3.4.)

a)

b)

c)

Fig. 3.4. Robotic cell components: a) – Robotic cell assembly, b) – Fanuc Arc Mate 100iBe welding robot, c) – Fronius TPS 4000 welding equipment.

Chapter 4. Experimental research on welding high-strength steels

4.1 Input data

Based on the findings from the current state-of-the-art analysis, the following research and development directions are considered relevant for optimizing welding technologies for high-strength steels.

The experimental program was designed to develop an optimal welding technology applicable to the high-strength steel S890QL, aiming to use it in the manufacturing of the "*rail welding equipment chassis*" assembly. The adoption of this new material over S355ML steel provides the advantage of reducing the assembly's overall weight.

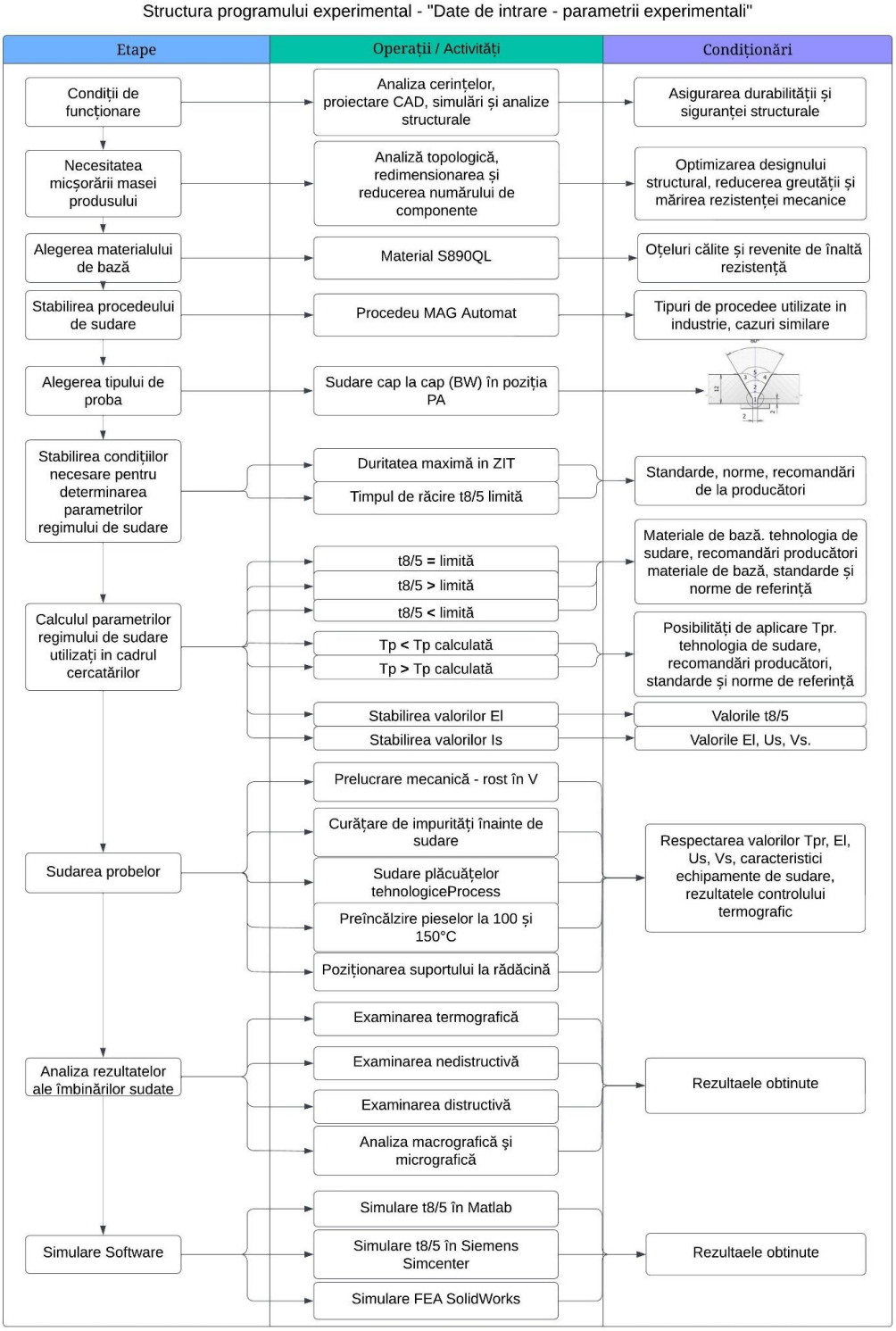

Fig. 4.1. Structure of the experimental program: "Input Data – Parameters"

4.2 Base material

The base material used for the experimental program was S890QL steel, a high-strength structural steel characterized by a guaranteed minimum yield strength of 890 MPa. This material offers an outstanding combination of strength and impact toughness, along with optimal machinability properties. It is an ideal choice for advanced supporting structures such as mobile cranes, loaders, trailer chassis, and agricultural equipment. Additionally, the material has superior bending capacity, excellent surface quality, high weldability, and guaranteed flatness, thickness, and bending properties.

The steel designation is as follows [127]:

- S - Construction steel;
- 890 - Minimum yield strength expressed in MPa;
- Q - Quenching and tempering;
- L - Low temperature;

The chemical composition of S890QL steel, from batch 629660, according to the quality certificate number 1220479001 (Appendix 1), as well as its equivalences with other types of steels according to different standards, are presented in Tables 4.1 and 4.2. The mechanical properties of the steel are provided in Table 4.3.

4.2.1 Calculation of weldability indices

Considering the influence of alloying elements on the base material properties (Chapter 1.2.4, according to Table 4.3.), the base material was purchased with a quality certificate 3.1 (Appendix 1), in accordance with the standard SR EN 10204:2005 [130]. Additionally, the material is accompanied by a quality certificate and delivery conditions, as per the standard SR EN 10025-6+A1:2023 [21]. The assessment of the risk of cold cracking, as well as the weldability of the base material, is carried out using the equivalent carbon content, the cold cracking index (PCM), and the hot cracking index (HCS) [129]. (Chapter 1.2.3.3 and Chapter 1.3.).

4.2.2 Determination of phase transformation temperatures

To determine the influence of preheating temperature on the structural transformations during the cooling of the weld bead deposited using the automated MAG welding process on S890Q steel, it is necessary to calculate the start and end temperatures of the martensitic transformation.

Transformation temperatures are critical for estimating the types of microstructures that will form upon cooling after welding and for determining the optimal preheating temperature in the welding process [131]. For non-alloyed or micro-alloyed steels, the main temperatures at which transformations occur during cooling, under conditions close to equilibrium (according to the Fe-Fe_3C diagram), are:

4.3 Selection of the welding process

To optimize the welding process for S890QL steel, the automated or robotic GTAW-MAG (Gas Tungsten Arc Welding – Metal Active Gas) processes represent one of the most effective technical and economic solutions. This welding process allows precise control of the welding parameters, which is essential to maintain the material's mechanical properties, such as tensile strength and toughness, which can be negatively affected by excessive temperature variations during the welding process.

4.5 Establishing the technological parameters of the welding regime

4.5.1 Determining the preheating temperature (T_{pr})

The metallurgical effects of preheating depend on the concentrated action of factors such as: cooling time $t_{8/5}$, the position of T_{pr} relative to M_s and M_f; the particular shape of the anisothermal and isothermal decomposition diagrams of undercooled austenite. In the case of steels with high welding requirements, it is necessary to know these parameters when establishing T_{pr}.

Following the application of methodology B in the SR EN ISO 1011 standard, the two values considered in the experimental research are: the maximum preheating temperature T_{prmax} = 150°C and the approximate minimum value T_{prmin} = 100°C.

These two preheating temperature values chosen for the experimental research correspond to the values prescribed by the manufacturers of S890QL steel [43, 134].

4.5.2 Calculations for estimating the limit values of cooling time between 800°C and 500°C ($t_{8/5}$)

Determining the limit value of the $t_{8/5}$ parameter, based on a maximum hardness requirement in the heat-affected zone (HAZ), in this case 450 HV10, helps in developing welding technologies that reduce the risk of cold cracking. The goal is to select welding regime parameters such that the cooling time t8/5 is greater than the calculated limit value, but within the limits set by the steel manufacturers.

For optimizing the welding technology, three distinct cases were considered:

- *Case 1 – $t_{8/5}$ = 8 s*: The welding technology respects the value of $t_{8/5}$, as indicated by the calculations. However, there is a risk of cold cracking and excessive hardening in the HAZ if the value accidentally falls below the required threshold;
- *Case 2 – $t_{8/5}$ = 12 s*: In this case, the welding technology respects the maximum value of t8/5, as recommended by the plate manufacturer. This is a limit case in which the welding technology results in a cooling time close to the critical value recommended by the manufacturers of S890QL material. Under these conditions, due to the combined action of certain objective factors, an accidental increase in grain size may occur, leading to a decrease in mechanical and toughness properties;
- *Case 3 – $t_{8/5}$ = 17 s*:

In this case, the recommendations for the value of $t_{8/5}$ are not followed, resulting in a cooling time exceeding the limit, which may cause an increase in grain size.

These cases are used to illustrate the impact of technological parameters on the material behavior in the HAZ and to optimize the welding process to reduce the risk of defect formation.

4.5.3 Determining the linear energy used in the welded specimens

To calculate the linear energy values, the cooling time equation (4.13) is used, according to [40]. Considering the input values in the experimental program for cooling time $t_{8/5}$ (8 s, 12 s, and 17 s), preheating temperature (100°C and 150°C), and material thickness (s = 12 mm) under two-dimensional propagation conditions, the linear energy value can be calculated using equation (4.14).

From the application of equation (4.14) and taking into account the $t_{8/5}$ and T_{pr} parameters, we obtain:

- Q=0,84 kJ/mm for $t_{8/5}$ = 8s and T_{pr} = 100°C;
- Q=0,72 kJ/mm $t_{8/5}$ = 8s and T_{pr} = 150°C;
- Q=1,03 kJ/mm $t_{8/5}$ = 12s and T_{pr} = 100°C;
- Q=0,88 kJ/mm $t_{8/5}$ = 12s and T_{pr} = 150°C;
- Q=1,23 kJ/mm $t_{8/5}$ = 17s and T_{pr} = 100°C;
- Q=1,04 kJ/mm $t_{8/5}$ = 17s and T_{pr} = 150°C.

4.5.4 Establishing the welding regime parameters

In order to simplify the research and enable quantitative and qualitative comparisons of the results obtained, welding speeds between 3…8 mm/s will be chosen, as recommended by the filler material manufacturer.

Based on the calculated linear energy values and considering the arc voltage and welding speed values selected, the welding current intensity required for the experimental stage is determined by applying the calculation formula (4.15) [40].

Tabel 4.1 Welding regime parameter values

Transfer mode	Specimen No.	T_{pr} [°C]	$t_{8/5}$ [s]	E_l [KJ/mm]	I_a [A]	U_a [V]	V_s [mm/sec]	V_a [m/min]	Transition thickness [mm]
SPRAY-ARC	1	100^{0}C	8	0,84	257	26	7	8.2	13.6
	2	150^{0}C	8	0,72	260	26	8	8.3	14.8
	3	100^{0}C	12	1,03	290	30	7	9.3	16.7
	4	150^{0}C	12	0,88	270	27	7	8.6	18.0
	5	100^{0}C	17	1,23	293	30	6	9.5	19.9
	6	150^{0}C	17	1,04	314	31	8	10.3	21.5
SHORT-ARC	7	100^{0}C	8	0,84	165	18	3	4	13.6
	8	150^{0}C	8	0,72	180	19	4	4.4	14.7
	9	100^{0}C	12	1,03	190	19	3	4.7	16.7
	10	150^{0}C	12	0,88	200	21	4	5.1	18.1
	11	100^{0}C	17	1,23	206	21	3	5.3	19.8
	12	150^{0}C	17	1,04	194	19	3	4.8	21.5

Following the calculation of the welding regime parameters, a model of the welding procedure specification was developed (Annex 3) [135].

4.6 Description of the experimental setup used for welding sample preparation

The experimental setup used for the welding of samples consists of:

- GMAW welding power source (FRONIUS TRANSPULS SYNERGIC 4000);
- Welding robot (FANUC ARC Mate 100iB);
- Temperature recording device with thermocouples (GRAPHTEC midi LOGGER GL200A);
- Infrared thermographic camera (FLIR E95);
- Oven for preheating the workpieces;
- Digital thermometer (GTH 1150).

The thermal field was visualized at both ends of the sample and in the middle of the joint area to ensure that the measurements were not influenced by phenomena occurring at the beginning and end of the weld bead.

The welding was performed in direct current with direct polarity using a MAG welding power source.

The experimental setup for welding the samples is shown in Figure 4.3.

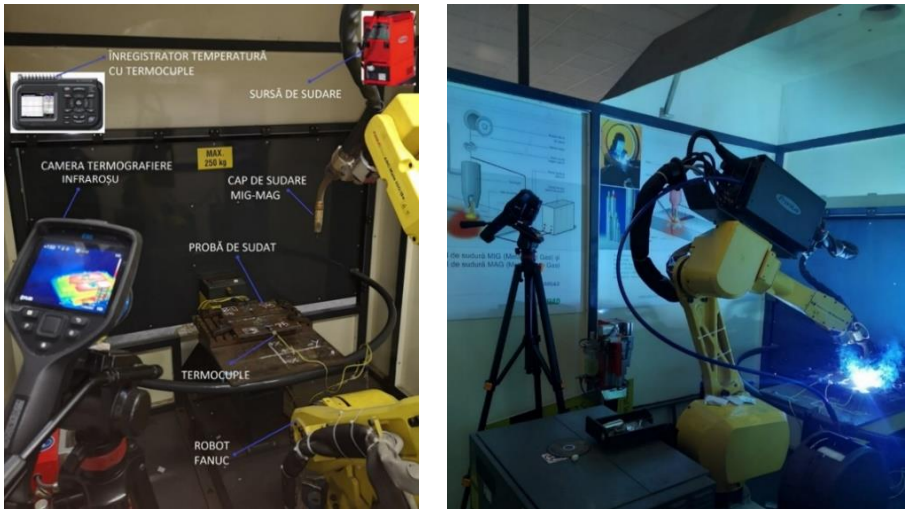

a) b)

Fig. 4.3. The experimental setup used for robotic MAG welding of the samples and for monitoring the welding process.

4.7 Experimental procedure [136]

In order to achieve the objectives established by the thesis topic, namely the analysis of welding possibilities for the high-strength steel S890QL, with the intention of using it in the construction of the railway track welding machine chassis, the experimental part was focused on three research directions:

- The first direction, which considers the cooling time $t_{8/5lim}$ for obtaining a maximum hardness of 450 HV10 in the Heat-Affected Zone (HAZ), analyzing three variants in which $t_{8/5}$: the first variant using $t_{8/5lim}$ = 8 s, the second variant where $t_{8/5}$ = 12 s is the maximum value recommended by steel manufacturers, and the third variant where $t_{8/5}$ = 17 s, a value exceeding the recommended limits;
- The second direction, which starts from the three previously presented cases, taking into account the preheating of the welded samples: the first case at a temperature of 100°C, the minimum value resulting from the calculation, and the second case at a temperature of 150°C;

  Note: It is mentioned that the preheating temperatures discussed in the experimental program correspond to practical situations encountered in the production of welded products used in the metal construction industry.
- The third direction, where for the six previously presented variants, the influence of changing the transfer mode (short-arc and spray-arc) is analyzed while keeping the other technological parameters constant ($t_{8/5}$, T_{pr}, E_l).

The experiments were conducted in accordance with the research directions outlined, respecting the parameters indicated in Table 4.7.

The experiments were designed in such a way that the obtained results could be implemented in industry, particularly in the case of root and fill layers made using the MAG welding process, and serve as an important foundation for developing new welding technologies in the analyzed field.

The dimensions of the samples used in the experiments were 150x300x12 mm.

4.8 Conclusions

In order to carry out the experimental program for analyzing the welding possibilities of high-strength steels (specifically S890QL steel), a total of 12 welded samples were made, considering the following technological parameters:

- *Preheating temperature (T_{pr})*: The preheating temperature was calculated using Method B, as described in the SR EN 1011-2:2002 standard, a methodology for preventing hydrogen-induced cracking in unalloyed steels with fine grain structure and low alloying content. According to the described methodology, the preheating

temperatures used for the welded samples were: T_{pr} = 100°C and T_{pr} = 150°C. The calculation of the preheating temperature values took into account the equivalent carbon content, diffusible hydrogen, and the material thickness used in the experimental samples (see § 4.5.1);

- *Cooling time between 800°C și 500°C ($t_{8/5}$)*: The cooling time $t_{8/5}$ was calculated considering the maximum hardness in the Heat-Affected Zone (HAZ), as well as the recommendations of high-strength steel manufacturers. The cooling time values used were: $t_{8/5}$ = 8 s, $t_{8/5}$ = 12 s, and $t_{8/5}$ = 17 s (see § 4.5.2);
- *Filler material transfer type*: short-arc transfer and spray-arc transfer;
- *Heat input*: heat input was calculated by substituting the parameters into the cooling time $t_{8/5}$ equation. After performing the calculations, the following linear energy values were obtained (see § 4.5.3):
  - Q=0,84 kJ/mm pentru $t_{8/5}$ = 8s and T_{pr} = 100°C;
  - Q=0,72 kJ/mm pentru $t_{8/5}$ = 8s and T_{pr} = 150°C;
  - Q=1,03 kJ/mm pentru $t_{8/5}$ = 12s and T_{pr} = 100°C;
  - Q=0,88 kJ/mm pentru $t_{8/5}$ = 12s and T_{pr} = 150°C;
  - Q=1,23 kJ/mm pentru $t_{8/5}$ = 17s and T_{pr} = 100°C;
  - Q=1,04 kJ/mm pentru $t_{8/5}$ = 17s and T_{pr} = 150°C.
- *Welding current intensity (I), arc voltage (U), and welding speed:* The welding parameters were chosen based on the linear energy value, the type of filler material transfer, and the recommendations of the additive material manufacturer. The parameters used in the experiments are presented in Table 4.7 (see § 4.5.4).

To eliminate the influence of the human factor on the quality of the welding process, the samples were made using a robotic GMAW welding process, ensuring precise control of the welding speed and consistency of the welding parameters over time.

Chapter 5. Experimental research on the analysis of welded samples

To evaluate the conformity of the welded samples and validate the designed welding technologies, the resulting welded samples were subjected to nondestructive examinations and destructive tests. The methods for analyzing the welded samples are presented in Figure 5.1.

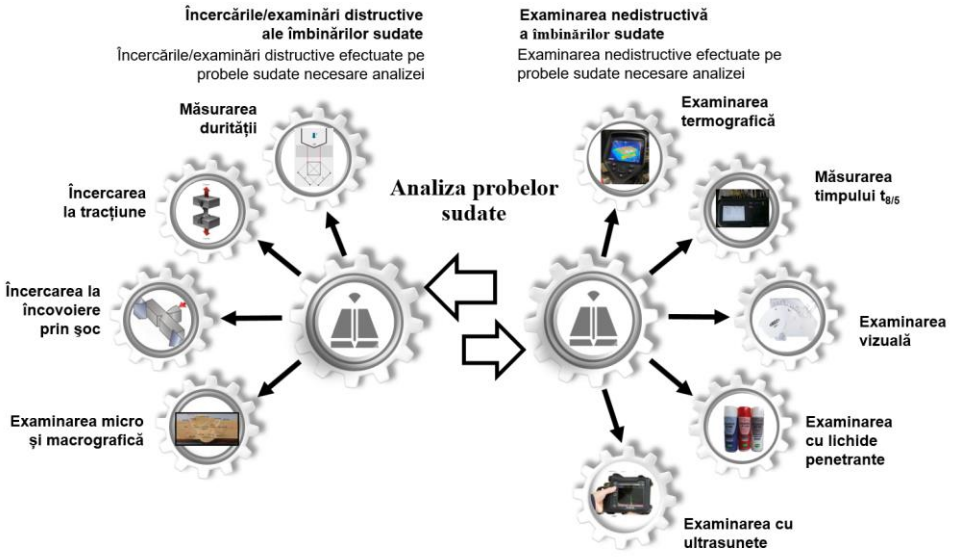

Fig. 5.1. Analysis of results for welded joints made of S890QL material

5.1 Estimation of the t8/5 parameter values and analysis of the thermal field during welding

The thermal cycle during welding influences the heat distribution in the welded components as well as the phase transformations occurring during the solidification of the molten metal pool [137, 138]. Monitoring the thermal field in welding processes is necessary to ensure compliance with the welding technologies and critical parameters such as preheating temperature (T_{pr}) and cooling time between 800°C and 500°C ($t_{8/5}$), among others [138].

For monitoring the thermal field on the surface of components, both contact methods (e.g., contact thermometers or thermocouples) and non-contact methods (e.g., pyrometers or infrared thermographic cameras) can be used [141, 144]. Recently, thermographic systems have increasingly been employed for temperature distribution measurements and welding process control. Infrared cameras, in particular, have been widely utilized for real-time studies of the welding process [145..148], enabling non-contact measurements and providing results with high accuracy and precision. The data collected by the camera offers insights into various aspects of welding outcomes, such as temperature distribution, geometric shape of the welded joints, and potential imperfections. The temperature data recorded by the camera can also be used to calculate cooling times within the range of 800–500°C, during which phase transformations occur in the material, affecting its microstructure and mechanical properties.

5.2 Estimation of the $t_{8/5}$ parameter values using contact thermocouples

Experimental measurements of the thermal field were conducted using thermocouples attached to the machined surface of the components, specifically in the heat-affected zone. The recorded temperature values were acquired using the Graphtec midi Logger GL200A equipment (Figure 5.2). The temperature variation of the thermal cycle during the welding processes for the 12 test specimens is presented in Figures 5.3..5.14. Based on the temperature variation, the cooling time $t_{8/5}$ can be measured for each specimen to verify the accuracy of the selected welding technology parameters. The measured values are summarized in Table 5.1.

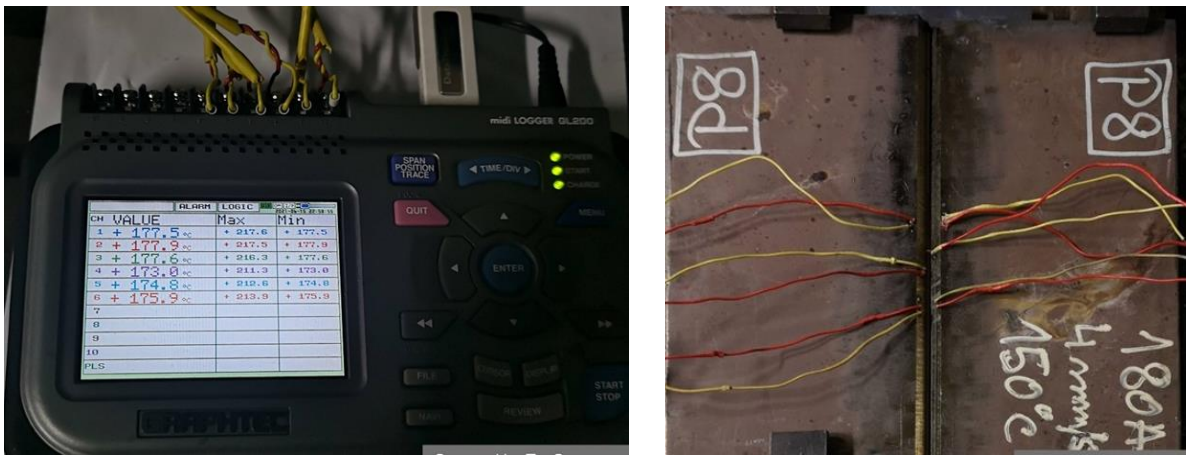

Fig. 5.2. Measurement of temperature values in the welded joint areas

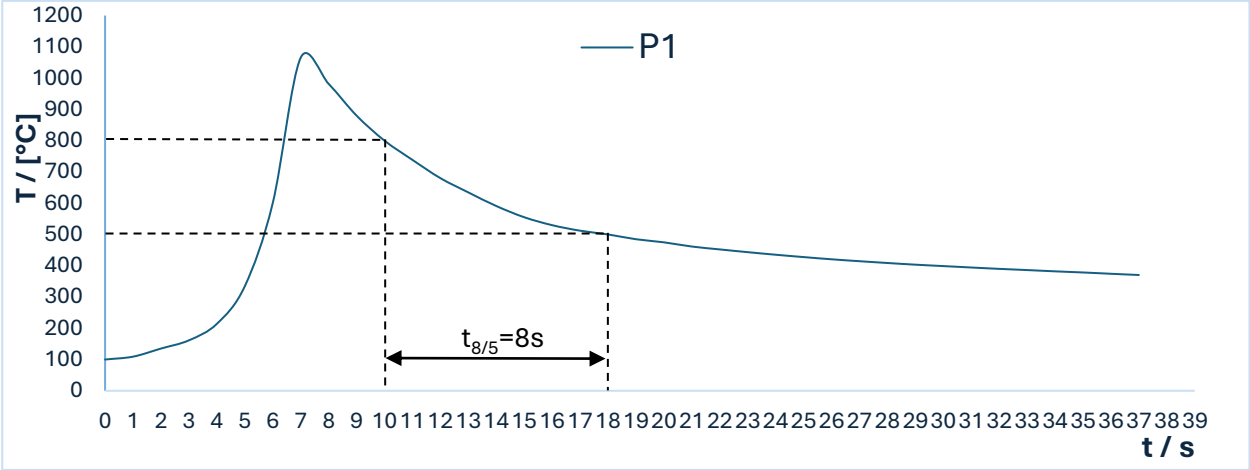

Fig. 5.3 Temperature variation of the thermal cycle for sample P1

Tabel 5.2 Cooling time values $t_{8/5}$

Nr. crt.	Arc transfer mode	Specimen Code	Imposed $t_{8/5}$ [s]	Measured $t_{8/5}$ [s]	Difference [s]	Deviation [%]
1.	Spary-arc	P1	8	8,0	0	0
2.		P2		8,1	0,1	1.23
3.		P3	12	12	0	0
4.		P4		12,1	0,1	0.82
5.		P5	17	16,9	- 0,1	0.59
6.		P6		17,1	0,1	0.58
7.	Short-arc	P7	8	7,9	0,1	1.26
8.		P8		8,1	0,1	1.23
9.		P9	12	11,8	-0,2	1.69
10.		P10		12	0	0
11.		P11	17	17	0	0
12.		P12		17	0	0

Following the analysis of the values presented in Table 5.1, it can be observed that in certain cases, there are slight differences between the calculated and measured $t_{8/5}$ cooling time values. The maximum differences observed were t = -0.2 s, representing a variation of 1.69%. These discrepancies between the imposed and measured t8/5 parameter values may be attributed to measurement errors or the specific conditions under which the experimental research was conducted.

5.3 Estimation of the $t_{8/5}$ parameter values and thermal field analysis during welding using infrared thermography [149]

During the experiments, the thermal cycle associated with the welding process was monitored using the FLIR E95 infrared thermography camera (Section 3.1.2). This setup enabled the practical determination of specific thermal parameters, such as the t8/5 cooling time, and provided a detailed representation of the thermal field distribution across the entire surface of the welded piece and throughout the entire welding process.

The use of an infrared thermography camera offers an overview of the thermal field of the joint with the advantage of monitoring the entire area of interest in a single recording.

Figures 5.15.a and 5.15.b illustrates thermographic images captured during the welding process, while Figure 5.15.c illustrates the temperature distribution along the weld seam at a specific moment after the process began. By continuously tracking the welding speed and elapsed time, the position of the point of interest and its corresponding temperature can be determined at any given moment.

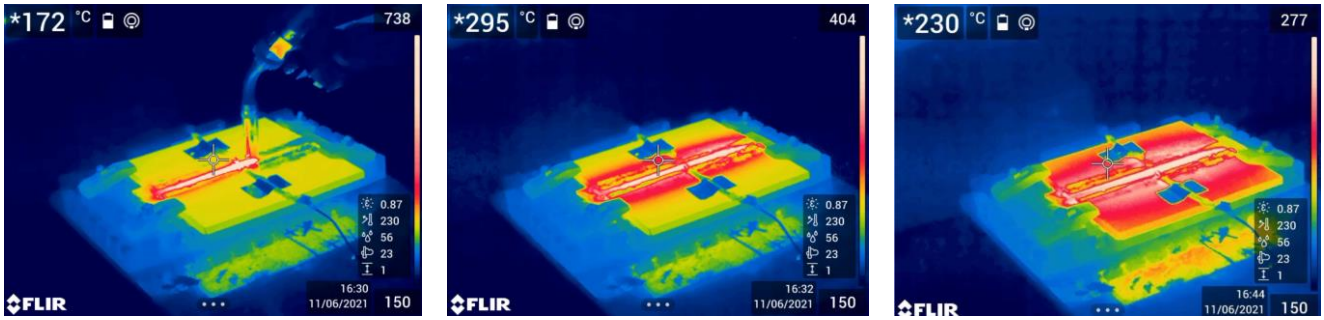

a) b) c)

Fig. 5.15. Thermal field distribution during welding proces

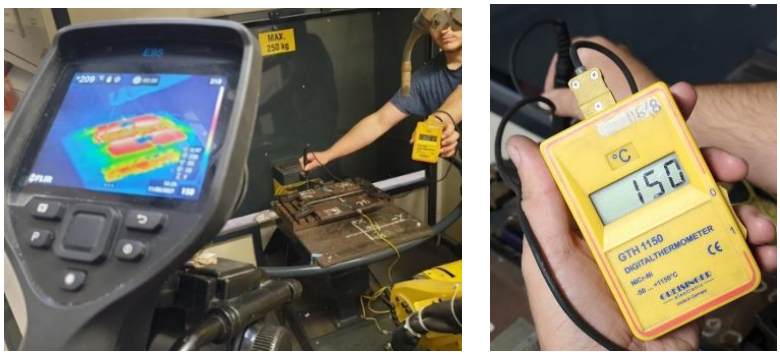

a) b)

Fig 5.16. Calibration of the infrared thermography camera using the contact thermometer: a) – infrared thermography camera, b) – digital contact thermometer.

To achieve the distribution of temperature values obtained from the images captured using the infrared thermography camera, a specialized application was developed in Matlab (version R2017a) that is capable of "reading" each image from the recorded video file and analyzing it in terms of temperature. The application generates a thermal distribution map. Using this application, researchers can accurately assess temperature values during the welding and cooling processes and identify potential problem areas, thus contributing to the improvement of the quality and reliability of the welds.

Based on the temperature values presented in Table 5.2, graphs of the temperature variation for samples P1 and P2 were plotted, using the thermocouples (P1, P2) and the infrared thermography camera (P1IT, P2IT), as shown in Figure 5.17.

5.4 Nondestructive examination of welded joints

Nondestructive examination plays an important role in evaluating the quality of welded joints, providing valuable information about the structural integrity without compromising the tested component. For this study, several nondestructive testing methods were applied (visual inspection, penetrant testing, and ultrasonic testing), followed by the collection of samples for destructive testing.

These methods were selected for the experiments to ensure a complete and detailed evaluation of the quality of the welded joints, providing both surface and volumetric inspections.

5.8 Macroscopic and microscopic analysis of welded joints

5.8.2 Macroscopic and microscopic examination

The optical macroscopic and microscopic examination was conducted in the LAMET Laboratory, in accordance with SR EN ISO 17639:2022 [165, 166].

The micrographic and macroscopic examinations were performed using the OLYMPUS GX51 optical microscope and the Quanta Inspect S scanning electron microscope (SEM).

Macroscopic and microscopic examination of sample P1

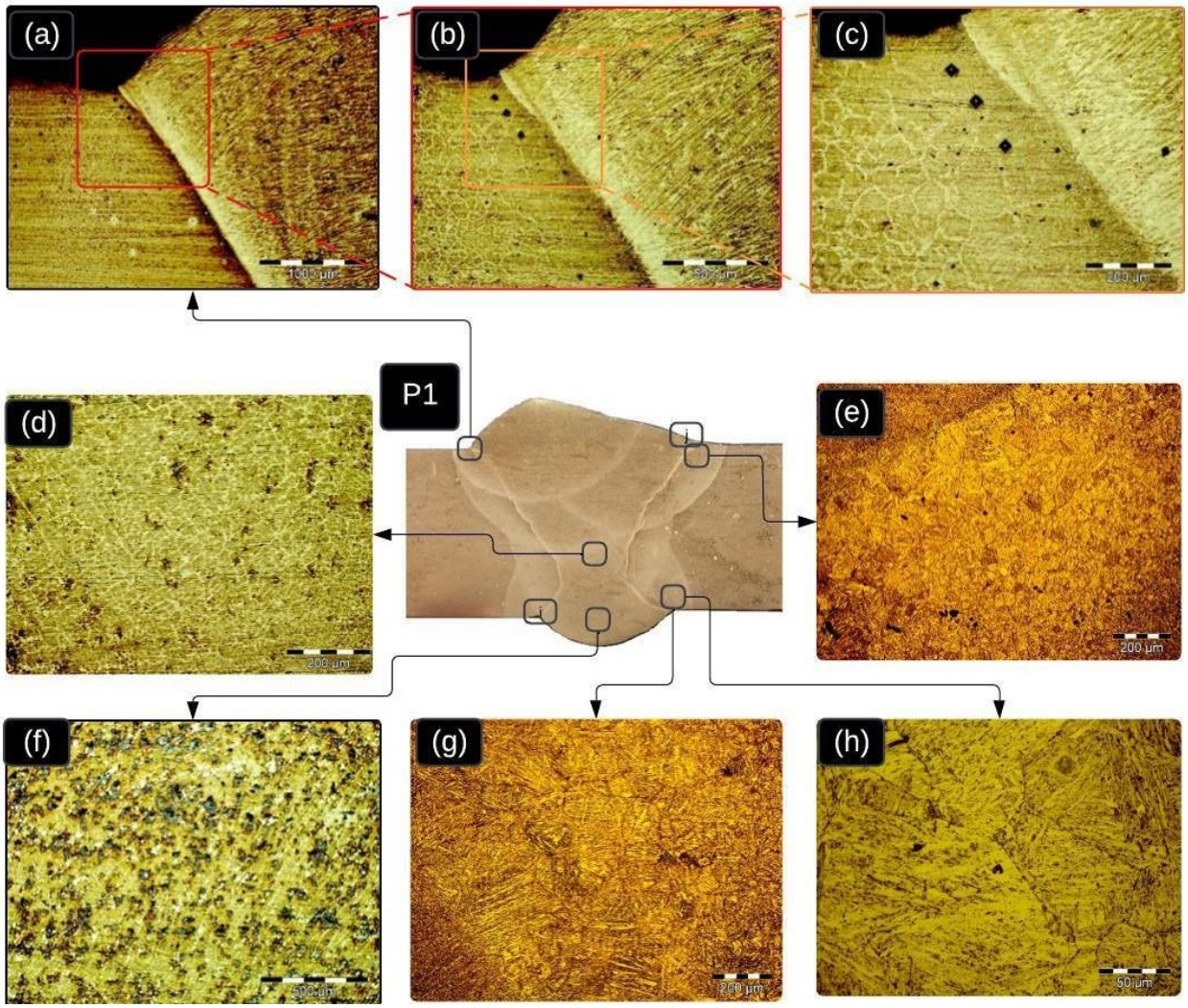

Fig. 5.41. Analysis of the microstructure of sample P1

a) Transition zone between the weld bead and the base material, at the surface of the weld, 50x.
b) Macroscopic analysis of the transition zone between the base material and the weld: A continuous fusion line is observed, without imperfections, and grain growth in the HAZ (Heat-Affected Zone), 100x.
c) Detail of the transition zone between the weld and base material in the HAZ, 200x.
d) The weld: Fine dendritic microstructure in chains, 200x.
e) Microstructure of the upper HAZ of the weld: Coarse martensite grains and residual austenite, 200x.
f) Microstructure of the weld in the root zone, 100x.
g) Detail of the microstructure in the root HAZ: Coarse martensite grains and residual austenite, 200x.
h) Detail of the HAZ: Coarse martensite grains and small areas of residual austenite, 1000x.

Residual austenite forms when cooling is faster than equilibrium cooling, as the transformation time is too short. Residual austenite tends to revert to ferrite and pearlite during subsequent reheating (thermal treatment, local weld repairs), generating internal stresses that are sufficiently large to cause cracking. Similarly, martensite and bainite can revert to ferrite/pearlite if the M_s or B_s temperatures are exceeded (the upper transformation temperatures, calculated in § 4.4.2). The Ms value for the analyzed

steel (S890QL) is 405°C, which can easily be reached during reheating for the deposition of subsequent layers.

5.9 Welding Procedure Qualification Records

Based on the analysis of the results obtained from the experimental investigations, procedure qualification records were written for two welding technologies: the first procedure is based on short-arc transfer welding for plates with a thickness of less than 8 mm, and the second on spray-arc transfer welding for plates with a thickness greater than 8 mm (Annex 7).

5.10 Conclusions regarding the welding of high-strength steels

- ✓ Monitoring the thermal field during the welding of high-strength steels can be done both using contact thermocouples and with an infrared thermography camera;
- ✓ In the case of measuring welding process temperatures using contact thermocouples, $t_{8/5}$ cooling time values were obtained with a maximum variation of 1.66% compared to the calculated values, leading to the conclusion that the technological requirements of the welding process were met;
- ✓ When monitoring the thermal field with an infrared thermography camera, the differences between the t8/5 parameter values determined by thermography and those based on mathematical formulas fall within acceptable ranges, with errors of up to 2.75% from the calculated $t_{8/5}$ time;
- ✓ Monitoring the thermal field during welding with infrared thermography constitutes a suitable tool for establishing the temperature distribution on the surface of the analyzed sample, as well as for measuring the $t_{8/5}$ parameter;
- ✓ Hardness measurements in characteristic zones highlighted an increase in hardness values in the weld bead or the heat-affected zone (HAZ), reaching a maximum value of 391 HV0.2, which is below the maximum limit imposed by current standards;
- ✓ The results obtained from tensile testing showed that the specimens failed at a rupture strength value below R_m=940 MPa (the minimum guaranteed value for S890QL steel) for specimens with a preheating temperature of T_{pr}=100°C. This leads to the recommendation to use a preheating temperature of T_{pr}=150°C;
- ✓ The yield strength values of the welded specimens exceed the minimum guaranteed limit of $R_{p0.2}$=890 MPa in all cases where a preheating temperature of T_{pr}=150°C was used;
- ✓ For the preheating temperature of T_{pr}=100°C, values below the minimum guaranteed $Rp_{0.2}$ value, or very close to it, were obtained. Therefore, the recommendation is to use a higher preheating temperature;
- ✓ The $t_{8/5}$ values considered in the experimental program do not lead to excessive hardening in the weld bead zones (which could result in cracking), nor overheating that would cause a loss of mechanical properties.

Conclusions regarding the influence of welding parameters, cooling times, and linear energy on the microstructure and results of destructive testing of samples P1-P12:

1. Fusion line quality:

- In all analyzed samples, the fusion line between the base material and the weld is continuous, with no visible imperfections at the macroscopic level. This indicates a high-quality welding process, ensuring structural integrity.

2. Heat-affected zones (HAZ):

- The weld microstructure consistently shows fine dendritic formations aligned along the thermal flow direction, suggesting controlled solidification with an appropriate cooling rate to prevent internal defects.

- In the HAZ, an increase in grain size is observed, typical for regions exposed to high temperatures followed by cooling. This effect is more pronounced in the over-heated zones.
- In all samples, the HAZ exhibits coarse martensite grains associated with high temperatures and rapid cooling. These grains can influence the strength and fatigue behavior of the weld.
- Coarse martensitic transformations are often observed in the transition and root zones, indicating thermal conditions that favor incomplete austenite-martensite transformations.
- In some samples (e.g., P3), carbide precipitates at the grain boundaries were identified, which may contribute to increased hardness but also to potential embrittlement of the HAZ.

3. Weld structure:

- In the root zone, the microstructure presents acicular dendritic formations oriented along the thermal flow direction, with potential for the formation of columnar grains oriented along the cooling direction. Small precipitate phases are also observed, which may contribute to local hardness increases.

4. Fillet angles:

- The fillet angles between the weld and the base material range from 122° to 178°, indicating a broad distribution of geometric conditions. Larger angles (e.g., 178° in P4) suggest significant overbeading of the weld, which may influence residual stresses and mechanical performance.

5. Base material:

- The base material structure consists of polyhedral ferrite and pearlite grains, typical for thermomechanically rolled material. At the interface with the HAZ, the grains become elongated due to thermally induced transformations.

6. General conclusion:

- The microstructure of the analyzed samples is generally uniform, with no defects, suggesting the use of a controlled welding process. However, careful monitoring of the HAZ is recommended to minimize coarse grain formation and improve phase transitions.
- The fillet angles and the distribution of precipitates should be correlated with mechanical testing to confirm compliance with applicable standards.
- In samples welded with lower preheating temperatures, acicular martensite and residual austenite are present, with a tendency for coarse grain formation in the HAZ as the cooling time increases. The cooling time ($t_{8/5}$) significantly influences the final weld structure. In samples with short cooling times (P1, P2, P7, P8), the weld microstructure is predominantly dendritic, with fine and uniform shapes. In contrast, samples with longer cooling times (P3, P4, P6, P10) exhibit a coarser and less homogeneous microstructure, with carbide precipitates in the HAZ and larger grain size. This suggests slower cooling that favors precipitation and grain growth.

Chapter 6. Theoretical and experimental research on CFD-FEM modeling in high-strength steel welding

A current trend in manufacturing processes is the minimization and/or elimination of non-productive times in the manufacturing flow, including those allocated for preliminary testing of the produced products and the developed technologies. To achieve this goal, one of the widely used methods is simulating real working conditions with the help of specialized software packages [168].

Modeling manufacturing phenomena and processes is a challenge that has become possible due to the development of new calculation techniques and algorithms, as well as the advancement of hardware components in computer structures. The Computational Fluid Dynamics (CFD) method plays an extremely important role in the design and verification of various projects involving fluid flow and heat transfer, eliminating the need for the experimental phase, at least in certain stages of development, which was previously indispensable. CFD analysis provides detailed information regarding the distribution of

velocity, pressure, temperature, or other relevant fluid parameters in transient or steady-state conditions [167].

For simulating the thermal cycle in welding, FEM offers a series of advantages, including:

- Multiple discretization options for the analyzed model, allowing easy analysis of phenomena occurring in the weld bead and its adjacent areas;
- The ability to define different material characteristics for the materials used in the simulation;
- It allows for the interpretation and visualization of the thermal field resulting from welding;
- It enables approximation of the stress and deformation levels in the welded components.

6.1 CFD simulation of cooling time $t_{8/5}$

6.1.1 Input data for modeling the thermal field during welding

- Base material: S890QL steel plate with dimensions 300 x 150 x 12 mm (Figure 6.2);
- Steel supporting plate with T-slot, dimensions 350 x 360 x 20 mm (Figure 6.3);
- Fixed-length weld bead: 300 mm (Figure 6.4);
- Moving welding pool;
- Ceramic support for root support (under the weld, between the steel plates and the T-slot plate).

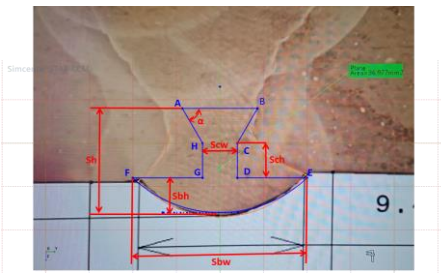

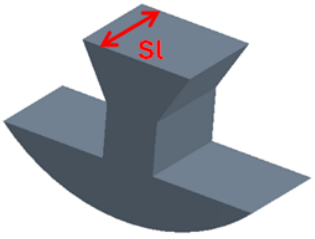

s_h [mm]	7
s_l [mm]	3.5
s_{bh} [mm]	2
s_{bw} [mm]	10
s_{ch} [mm]	2
s_{cw} [mm]	2
α [^{0}C]	60

Fig.6.4. Geometric elements of the weld bead

6.1.2 Materials used for the experiments

The definition of the characteristics of the materials used was based on the chemical composition and the welding process temperature. The characteristics of the materials used are presented in Table 6.1.

For the simulation of the thermal field during welding, the welding technology used in sample P1 (Table 6.2) was considered.

Figure 6.8 shows the distribution of the thermal field generated by the welding source at the beginning of the welding process (Figure 6.8.a), at the midpoint of the process (Figure 6.8.b), and at the end of the process (Figure 6.8.c).

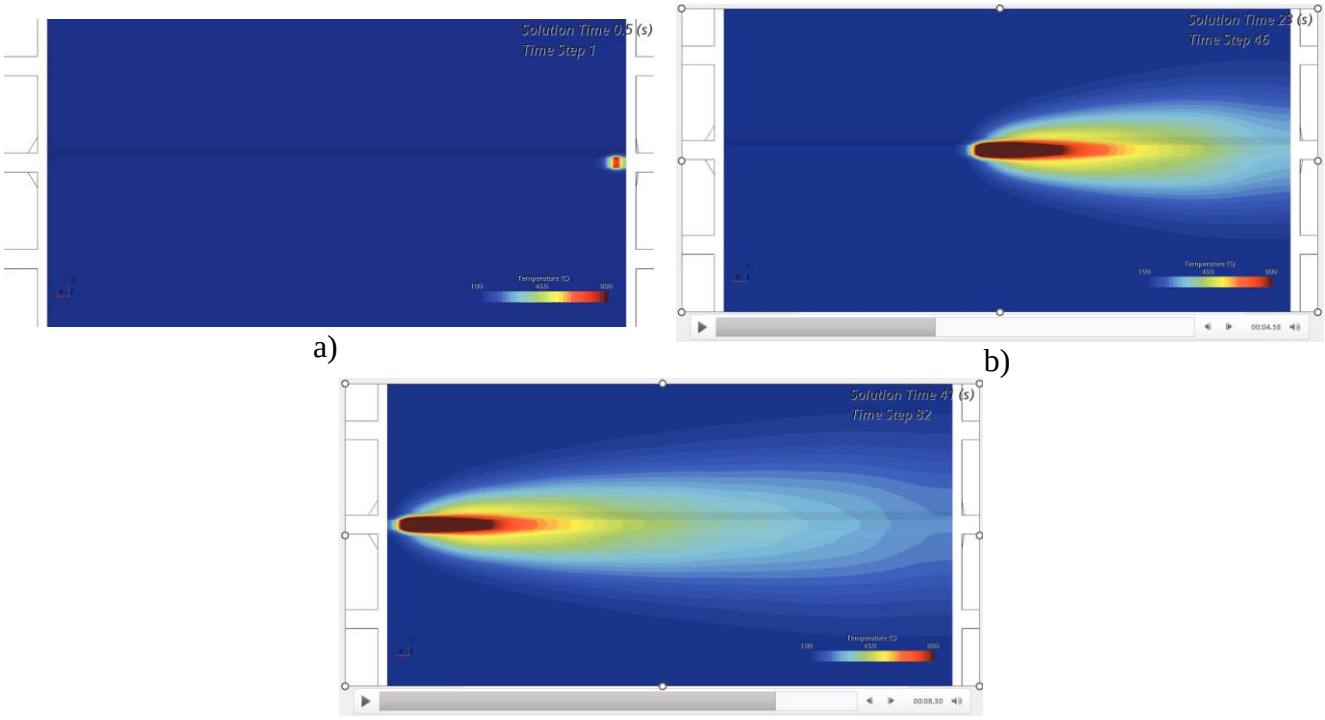

Fig 6.8. Simulation of the Thermal Field Distribution of the First Layer (Root) for Sample P1: a) – at the beginning of the welded sample – t = 0.5 s; b) – at the midpoint of the weld bead – t = 23 s; c) – at the end of the weld bead – t = 46 s.

6.1.4 Validation of simulation model results

The validation of the simulation model involves comparing the simulation results with the temperature measurement data obtained using contact thermocouples. Figure 6.9 shows the temperature variation for the two components at measurement points 1 and 2. Based on the temperature variation, the $t_{8/5}$ values for the two components were extracted, and these values are presented in Table 6.3. It can be observed that the $t_{8/5}$ values obtained from the simulation are $t_{8/5}$-1 = 7.57 s and $t_{8/5}$-2 = 7.58 s, with a measurement error of 5.25% and 5.37%, respectively.

6.2 Influence of base material modification on chassis assembly characteristics

Given the differences in the mechanical properties of S355ML and S890QL materials, it was proposed to modify the thickness of the reinforcement elements of the main chassis frame without altering its overall dimensions. Modifying the overall dimensions of the chassis and its components requires a detailed and complex analysis of the entire welding equipment for the railway track rails.

After redesigning the chassis by replacing the base material and modifying the component thicknesses, a comparative FEM analysis was performed, considering both the changes in the base material properties and the modification of the material thickness in some of the components.

To analyze the mass difference of the chassis resulting from the base material modification and component thickness change, a 3D model of the chassis was created in SolidWorks design software.

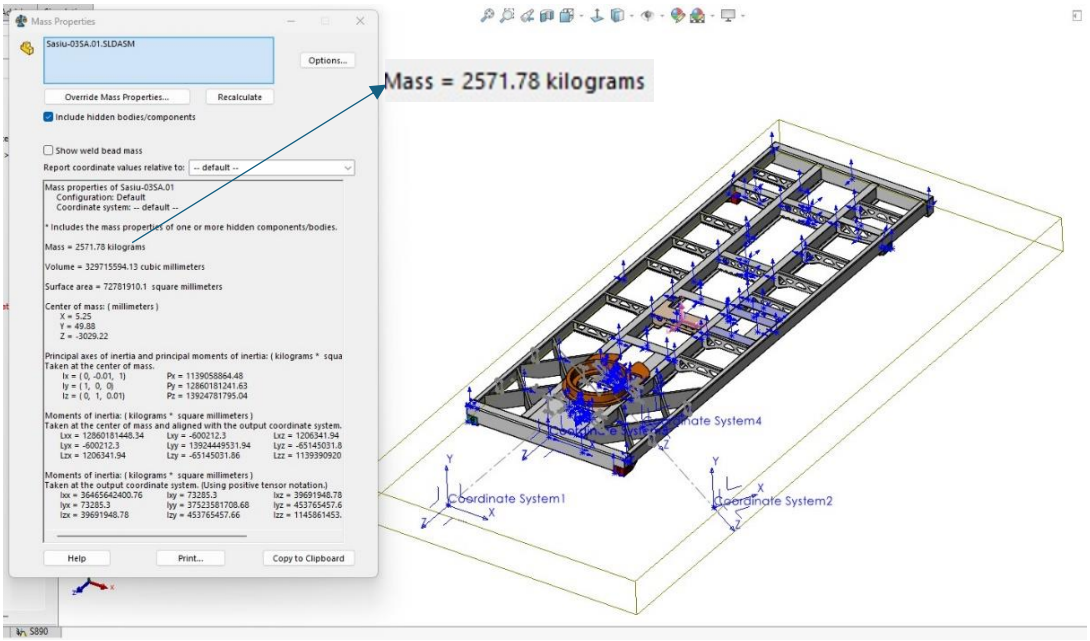

Fig.6.10. Determination of the chassis assembly mass made of S355ML steel.

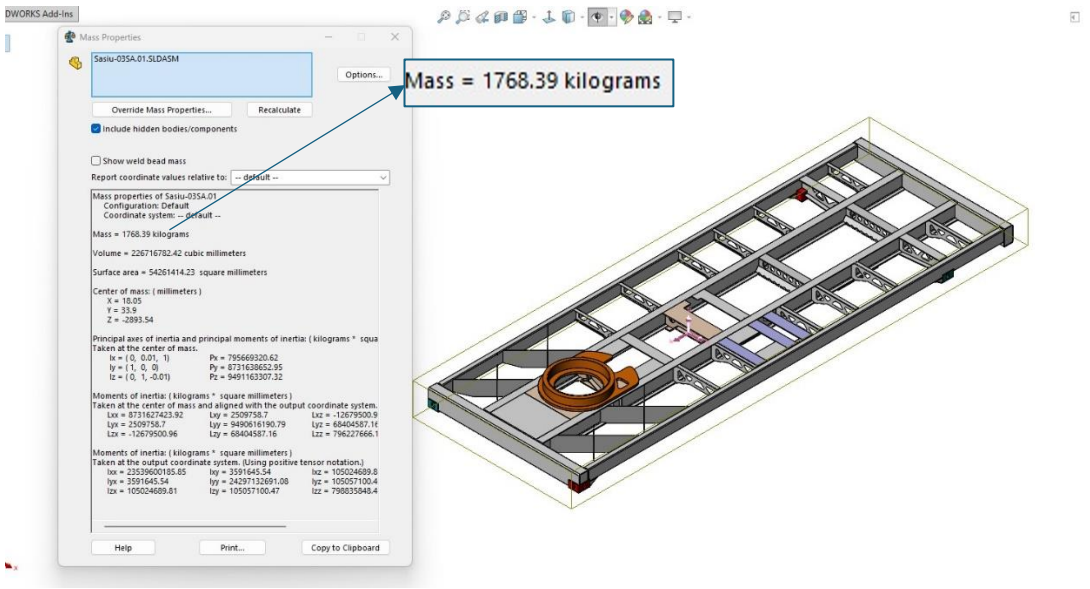

Fig.6.11. Determination of the chassis assembly mass made of S890QL steel.

From the analysis of figures 6.10 and 6.11, it can be observed that, following the modification of the component thicknesses presented in table 6.4, the mass of the chassis assembly decreased from 2571.78 kg to 1768.39 kg. The analysis of the values shows that the chassis mass was reduced by 803.39 kg, which represents a 31.23% reduction from its initial mass.

6.3 FEM simulation of the welding machine chassis

For the simulation process, using the specialized software SolidWorks, the stresses resulting from the use of the welding head were considered. The stresses applied to the chassis model were: 5000 kgf, representing the mass of the welding head (longitudinally along the chassis or at a 60° angle to the chassis's longitudinal axis), and 2800 kgf, from the mass of the welding head clamping device.

The purpose of using high-strength steels in such applications is often to reduce weight by decreasing the thickness of components. Reducing the structural weight brings numerous advantages, including reduced material consumption, fewer welding operations, and lower transportation costs..

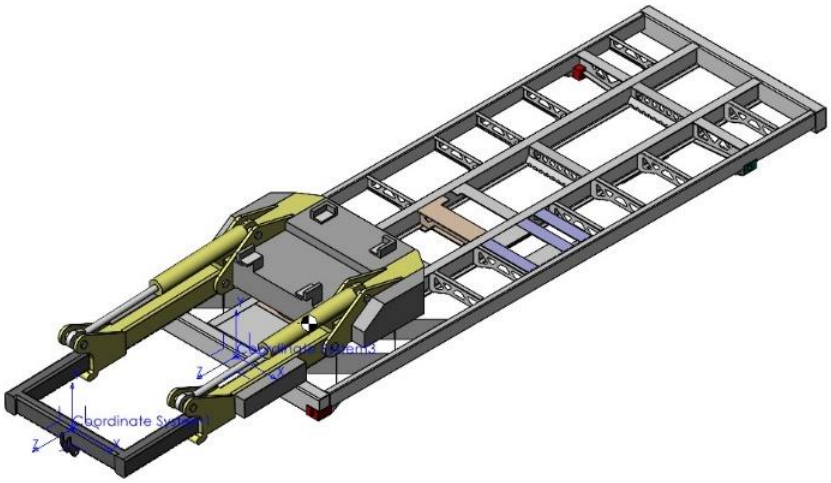

a)

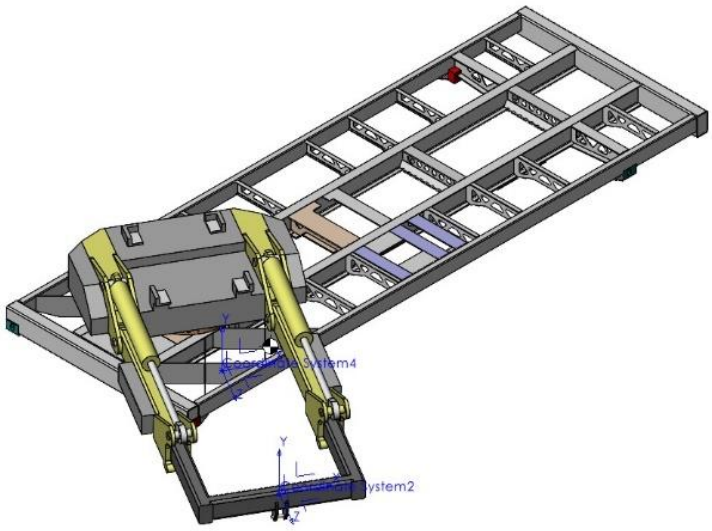

b)

Fig.6.12. 3D model of the chassis: a) – in the displacement position; b) – in the operating position.

6.3.1 General loads and constraints of the study

According to the assembly and operating model, the chassis will have fixed attachment points on the welding machine body, which are located at its corners (Figure 6.14).

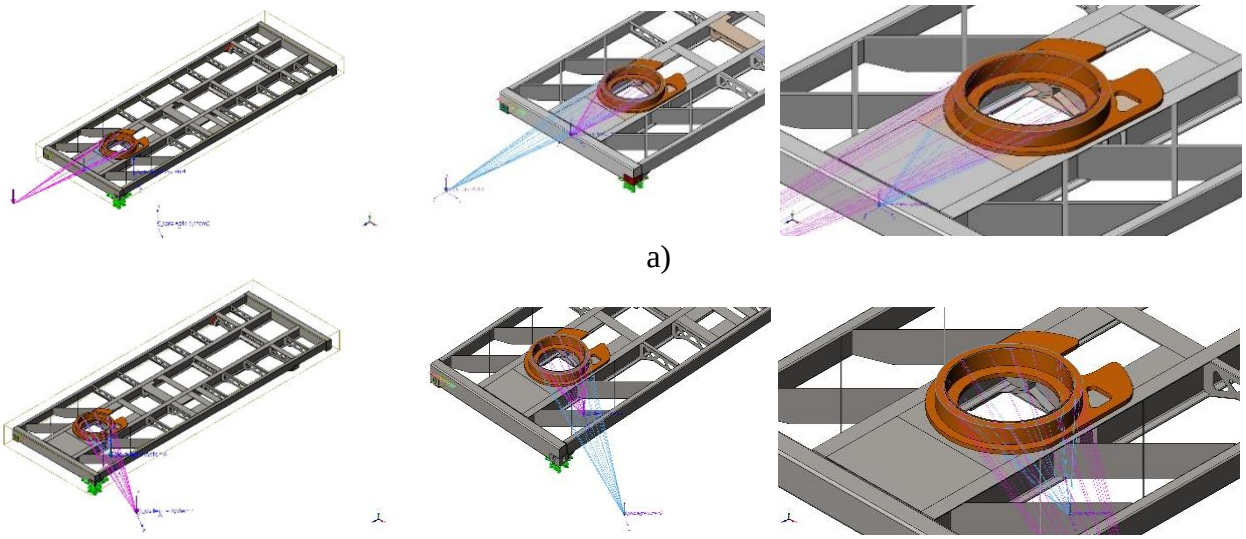

a)

b)

Fig.6.15. Chassis loading mode: a) – applying loads along the chassis; b) - applying loads at an angle of 60° to the longitudinal axis.

6.3.2 Simulation of the chassis made of S355ML material with the load applied at a 60° angle to the longitudinal axis of the chassis.

Name	Type	Minimal value	Maximal value
Tensions	von Mises tensions	0.000N/mm^2 (MPa) Nod: 292859	274.545N/mm^2 (MPa) Nod: 348380

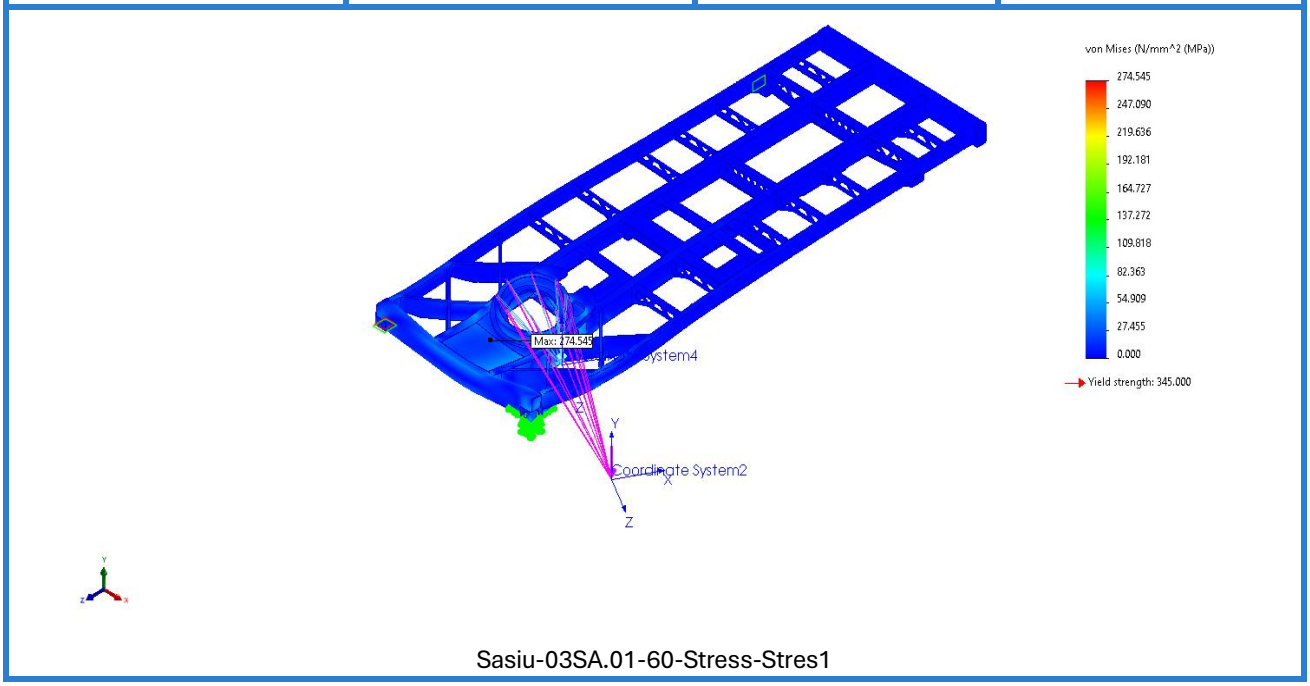

Fig.6.24. Distribution of von Mises stresses for the S355ML material with the load applied at a 60° angle to the longitudinal axis of the chassis.

Name	Type	Minimal value	Maximal value
Tensiune echivalentă	ESTRN	0.000 Element: 145348	0.000 Element: 171834

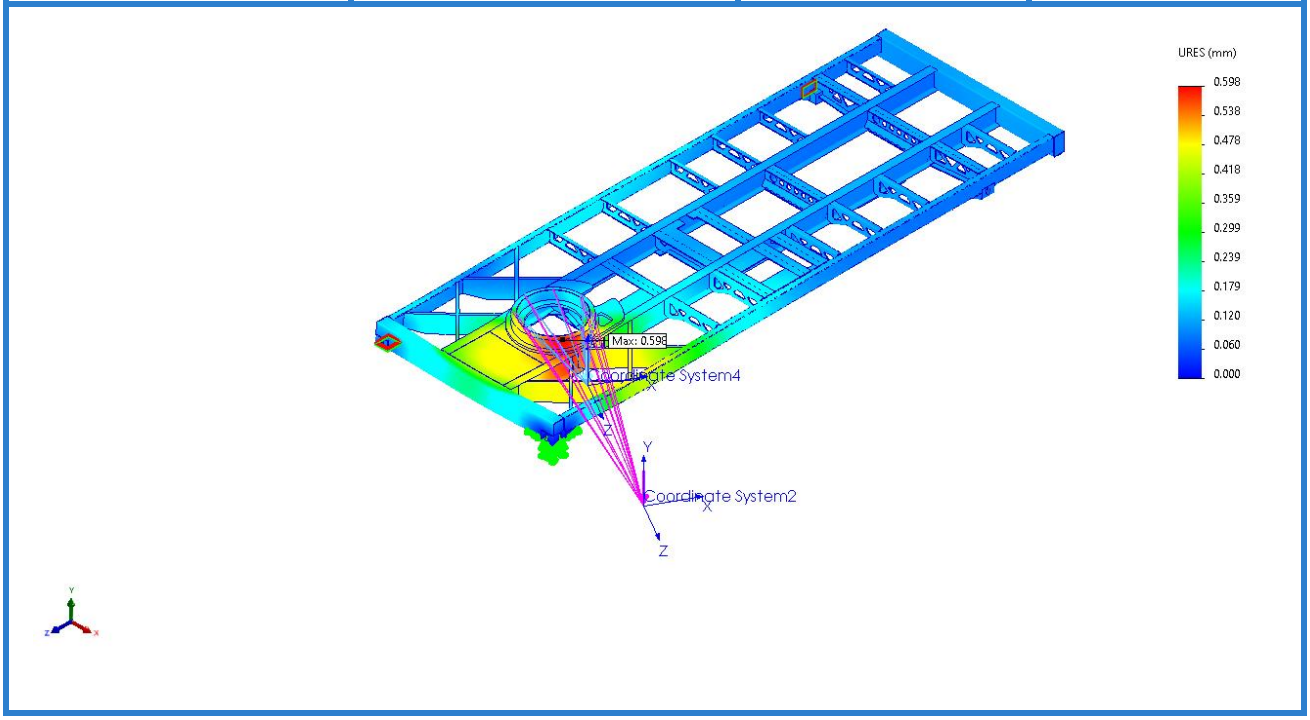

Fig.6.25. Distribution of displacements for the S355ML material with the load applied at a 60° angle to the longitudinal axis of the chassis

Nume	Tip	Valoare minimă	Valoare maximă
Tensiune echivalentă	ESTRN	0.000 Element: 145348	0.000 Element: 171834

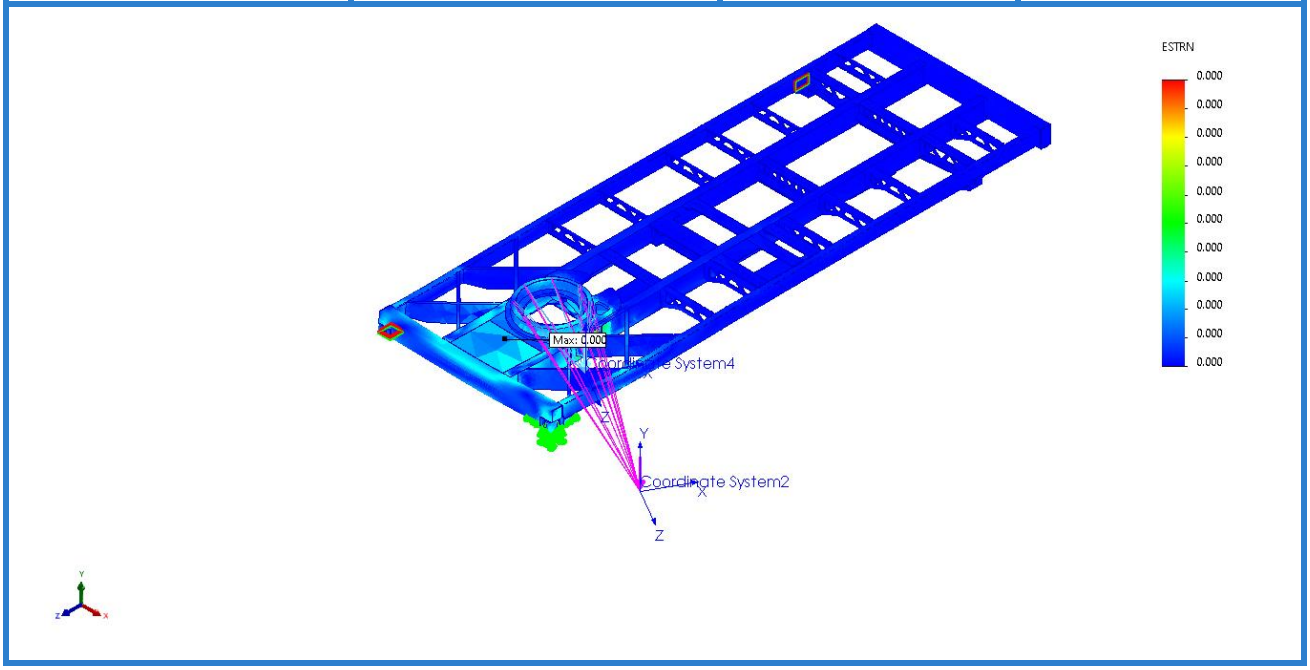

Fig.6.26. Distribution of equivalent stresses for the S355ML material with the load applied at a 60° angle to the longitudinal axis of the chassis.

Name	Type	Minimal value	Maximal value
Safety factor	Automated	1.257e+00 Nod: 348380	1.464e+05 Nod: 350933

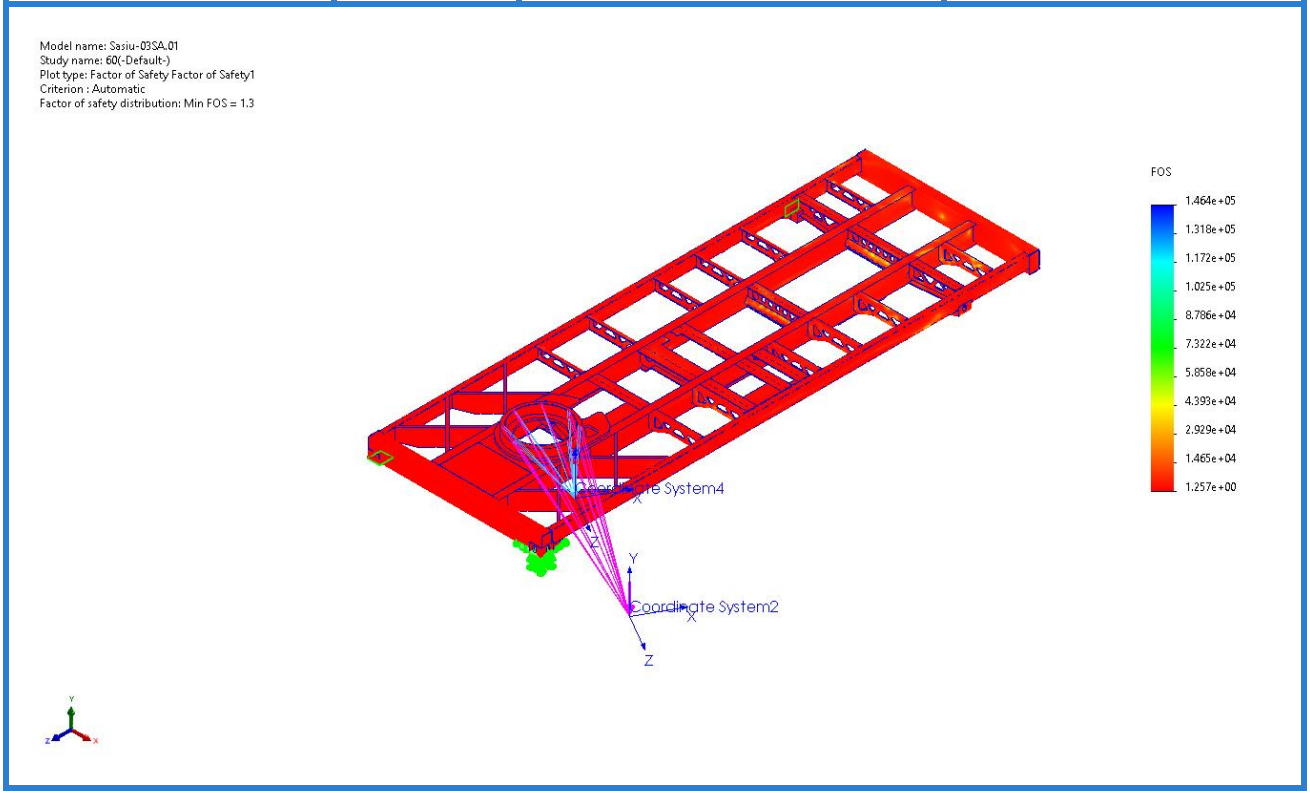

Fig.6.27. The distribution of the safety factor for S355ML material with the load applied at an angle of 60° to the longitudinal axis of the chassis.

6.4 Conclusions:

Modeling the thermal field during welding provides the opportunity to reduce the design times for welded structures. At the same time, it offers information regarding the temperature distribution during the welding process, as well as the ability to measure important parameters, such as the cooling time $t_{8/5}$.

The validation of the simulation model used in this doctoral thesis was carried out by comparing the temperature distribution curve during welding, obtained with the help of contact thermocouples, with that obtained through simulation, in order to determine the $t_{8/5}$ value. The values indicate a significant similarity in the temperature distribution and, implicitly, in the $t_{8/5}$ values. It can be observed that the $t_{8/5}$ values obtained from the simulation are $t_{8/5}$-1 = 7.57 s and $t_{8/5}$-2 = 7.58 s, with a measurement error of 5.25% and 5.37%, respectively.

From the comparative analysis of the results obtained through FEM, the following information regarding the stresses to which the welded structure is subjected during operation can be highlighted:

- Following the redesign of the chassis structure by replacing the S355ML steel with S890QL and using components with smaller thickness, the mass of the assembly is reduced by 31.23%;
- The reduction in the mass of the chassis allows for the use of a welding machine with a heavier welding head, but with superior functions in terms of technological parameters;
- In the case of using S355ML material for manufacturing the chassis, the maximum stresses during the operation of the installation approach the yield strength of the material, representing a risk of failure in the event of disturbing factors that increase the stresses accidentally;

- In the case of using S890QL steel, the stresses during operation reach up to 30% of the yield strength, which offers the possibility of using the installation under higher stresses and/or further reducing the thickness of the components;
- The safety factor increases when using S890QL steel to values over 2.991, which allows for additional loading of the welding installation without the risk of failure during operation;
- The deformations caused by the stresses to which the chassis is subjected reach a maximum of 0.946 mm, relatively low values that do not pose a risk to the operation of the welding installation.

Chapter 7. Final conclusions, original contributions, and future research directions

7.1 Conclusions from the theoretical research

From the theoretical analysis of the current state regarding the use of high-strength steels and their weldability, the following important conclusions were drawn:

- The development of high-strength steels (HSS) began in the mid-20th century, with the appearance of normalized steels with a tensile strength of 400…500 MPa (S355N/NL, S460NL/ML), reaching current values of 1400 MPa for ultra-high-strength steels (S1300Q - see § 1.2) or 1700…2000 MPa for advanced high-strength steels (MS 1250/1500);
- High-strength steels are used for their high mechanical properties, corrosion resistance, as well as for their fracture energy values at low temperatures, thus ensuring a significant reduction in the structural mass and their use in different environmental conditions (see § 1.3) ;
- With the development of this category of steels, they have found applications in various industrial fields: automotive (structural components), railway transport (transport tanks, infrastructure), offshore drilling platforms, shipbuilding, energy (wind turbines, transmission towers, and other energy-related structures), construction and infrastructure (buildings, bridges), and heavy equipment manufacturing (lifting equipment, excavators, bulldozers, and other excavation equipment) (see § 1.1) ;
- The weldability of high-strength steels is conditioned by the carbon content, as well as by the alloying elements, with equivalent carbon being a general criterion for analyzing the weldability of these materials (see § 2.2.1) ;
- The main issues regarding the weldability of high-strength steels are related to the risk of cold cracking (due to the formation of hard and brittle structures, the presence of internal stresses, and diffusible hydrogen) and the loss of toughness properties, manifested by a decrease in fracture energy under dynamic loading and an increase in the ductile-to-brittle transition temperature (caused by grain growth) (see § 2.1.3);
- For proper welding of high-strength steels, it is recommended to perform preheating (to avoid cold cracking) and to weld with stringer beads (to avoid grain growth) (see § 2.2.2);
- For welding joints in high-strength steels, most conventional fusion welding processes can be used, with special attention given to processes where heat dissipation is rapid (EBW and LASER), as there is a risk of hard and brittle structures forming and an excessive increase in mechanical properties in the HAZ and the welded seam (see § 2.3).

7.2. Conclusions from the theoretical research

Based on the experimental research conducted within the scope of this doctoral thesis, the following conclusions can be drawn:

- High-strength steels can be successfully used for welding various welded structures in the automotive and railway industries and can effectively replace currently used steels, with the aim of enabling the use of higher load-bearing capacities during operation and reducing the mass of the welded structure.
- Based on the welding technologies developed within the experimental program and the obtained results, a decision can be made to apply these technologies when using high-strength steels for welding structures.
- In the case of welded structures, based on the research results obtained in the thesis as well as the techno-economic analysis, a decision can be made to replace the old base materials with high-strength steels.
- Non-destructive testing (VT, PT, and UT) performed on welded samples did not reveal defects that would exclude the samples from the experimental set.
- Considering the importance of the cooling time $t_{8/5}$, for the practical verification of the calculated value, the experimental research demonstrated the possibility of measuring this value using contact thermocouples and infrared thermography.
- The hardness values of the welded samples did not exceed the maximum value allowed by the current standards, at which the risk of cold cracking is avoided, being minimal. The highest hardness value was 391 HV0.2, obtained for sample P5, which was welded with a preheating temperature of T_{pr} = 100°C. In certain areas of the weld and the HAZ, a variation of hardness values from 272 to 291 HV0.2 can be observed. The lower values are caused by grain growth due to overheating. Considering the issues encountered when welding high-strength steels, it is recommended to pay particular attention to selecting the preheating temperature-linear energy combination. Too low values may lead to over-tempering of the weld metal and HAZ, risking the formation of carbide precipitates, which increases hardness and the risk of cold cracking. Using high values can lead to overheating with a grain growth effect and a reduction in mechanical properties
- For the majority of welded samples with a preheating temperature of T_{pr} = 100°C, the tensile strength values were below the minimum guaranteed limit - R_m min = 940 N/mm², except for sample P11, where the R_m value was R_m = 951 N/mm².
- For the samples with a preheating temperature of Tpr = 100°C, the yield strength values ($R_{p0.2}$) were below or close to the minimum guaranteed limit, except for sample P11.
- The obtained values of the fracture energy from the shock bending test were above the minimum required by the current standards for S890QL material.
- Metallographic analysis performed in the areas of interest of the welded samples (base material, heat-affected zone, and weld bead) revealed that the fusion line between the base material and the weld is continuous, with no visible imperfections. The weld microstructure consistently displays fine dendritic formations aligned along the thermal flow direction. In all samples, the HAZ exhibits coarse martensite grains, associated with high temperatures and rapid cooling. In certain samples, an increase in grain size was observed in the HAZ, typical for regions exposed to high temperatures followed by cooling. This increase is more pronounced in the over-heating areas.
- In the thermal field modeling for welding, the obtained values indicate a high similarity in the temperature distribution and, consequently, in the $t_{8/5}$ values. It is observed that the $t_{8/5}$ values from the simulation are $t_{8/5}$-1 = 7.57 s and $t_{8/5}$-2 = 7.58 s, with a measurement error of 5.25% and 5.37%, respectively.

- From the comparative analysis of the results obtained using FEM, it appears that when using S355ML material for chassis manufacturing, the maximum stresses during the operation of the installation approach the material's yield strength limit, which represents a risk of failure if perturbing factors increase the loading conditions. When using S890QL steel, the stresses during the operation of the installation reach up to 30% of the yield strength, providing the potential for higher loading conditions and/or further reduction in component thickness. The safety factor increases when using S890QL steel to over 2.991, allowing for additional loading of the welding installation without the risk of failure during operation. The deformations caused by the stresses to which the chassis is subjected are a maximum of 0.946 mm, which are relatively low and do not pose a risk to the welding installation's operation.

7.3.Personal contributions

In light of the proposed objectives and the results of the theoretical and experimental research carried out during the development of this doctoral thesis, the personal contributions can be summarized as follows:

7.3.1. Theoretical contributions:

- Conducting a study on the current state of high-strength steels used in the manufacturing of welded structures, presenting their classification, evolution, and specific characteristics (see § 1).
- Carrying out an extensive study on the weldability of high-strength steels and presenting the main issues encountered with these steels (see § 2).

7.3.2. Experimental contributions:

- Development and implementation of the experimental program, including the realization of the 12 welded samples made of S890QL steel, using the robotized GMAW welding process (see § 3);
- Development of welding technologies, taking into account the recommendations of the standards in force, as well as the recommendations of manufacturers;
- Non-destructive examination of the resulting welded specimens by qualified operators (visual examination, liquid penetrant examination, ultrasonic examination);
- Carrying out mechanical tests in certified laboratories to determine the mechanical characteristics of each individual welded specimen (tensile test, micro-hardness determination, impact test);
- Performing microscopic and macroscopic examinations of the welded joints;
- - $t_{8/5}$ measurement and thermal field analysis using contact thermocouples and infrared thermography;
- Measurement of $t_{8/5}$ paramaeter and thermal field analysis using contact thermocouples and infrared thermography/
- Thermal field analysis using contact thermocouples and infrared thermography;
- Conduct experimental research on CFD-MEF modeling of high strength steels;
- Development of an experimental 3D model of the chassis to estimate stresses and strains during welding;
- Realization of an experimental stand for testing the chassis assembly fabricated by welding of S890QL steel fabricated parts;
- Realization of the welding technology approval reports for 2 welding technologies: first short-arc transfer welding, for sheet thickness less than 8 mm, second spray-arc transfer welding, for sheet thickness more than 12 mm.

- Development and execution of the experimental program, which included the fabrication of 12 welded samples made from S890QL steel using the robotic GMAW welding process (see § 3).
- Development of welding technologies, considering both the recommendations of current standards and those of manufacturers.
- Nondestructive examination of the welded samples with the assistance of qualified operators (visual inspection, penetrant testing, ultrasonic testing).
- Conducting mechanical tests in certified laboratories to determine the mechanical characteristics of each welded sample (tensile testing, microhardness determination, shock bending testing).
- Performing microscopic and macroscopic examinations of the welded joints.
- Measuring the $t_{8/5}$ parameter and analyzing the thermal field using contact thermocouples and infrared thermography.
- Conducting experimental research on CFD-FEM modeling for high-strength steels.
- Creating a 3D experimental model of the chassis for stress and deformation estimation during welding.
- Designing an experimental setup for testing a welded chassis assembly made from S890QL steel components.
- Preparing approval reports for welding technologies for two welding processes: short-arc transfer for plates with thicknesses under 8 mm and spray-arc transfer for plates thicker than 12 mm.

7.4.Future research directions

The theoretical and experimental results obtained through the scientific research program presented in detail in this doctoral thesis open the opportunity for further research in the following directions:

- Development of a prototype welding installation chassis using the new S890QL steel and approved welding technologies.
- Redesign of the chassis to reduce the thickness of the components and adapt the dimensional characteristics to the new operating conditions.
- Publication of unpublished results in scientific events, international conferences, and specialized journals.

Bibliography

[1]. Heavy-duty lightweighting - By SSAB, data publicării articolului, 25 October 2021, https://www.automotivemanufacturingsolutions.com/voice/heavy-duty-lightweighting/42417.article. (accesare la 18.06.2023.).
[2]. ***, SSAB AB , Suedia, High strength steel, https://www.ssab.com/en/brands-and-products/strenx (accesare la 28.10.2023).
[3]. Javidan, F., Heidarpour, A., Zhao, X.L., Hutchinson, C.R. and Minkkinen, J., Effect of weld on the mechanical properties of high strength and ultra-high strength steel tubes in fabricated hybrid sections. *Engineering Structures*, *118*, pp.16-27. 2016.
[4]. Haslberger, P., Holly, S., Ernst, W. et al. Microstructure and mechanical properties of high-strength steel welding consumables with a minimum yield strength of 1100 MPa. J Mater Sci 53, 6968–6979. 2018.
[5]. Tümer, M., Schneider-Bröskamp, C. and Enzinger, N., Fusion welding of ultra-high strength structural steels–A review. Journal of Manufacturing Processes, 82, pp.203-229. 2022.
[6]. Amraei, M., Dabiri, M., Björk, T. and Skriko, T., Effects of workshop fabrication processes on the deformation capacity of S960 ultra-high strength steel. Journal of Manufacturing Science and Engineering, 138(12), p.121007. 2016.
[7]. Guo, W., Crowther, D., Francis, J.A., Thompson, A., Liu, Z. and Li, L., Microstructure and mechanical properties of laser welded S960 high strength steel. Materials & Design, 85, pp.534-548. 2015.
[8]. Stadler, M., Schnitzer, R., Gruber, M., Steineder, K. and Hofer, C., Influence of the Cooling Time on the Microstructural Evolution and Mechanical Performance of a Double Pulse Resistance Spot Welded Medium-Mn Steel by Metals. 11(2), 270. 2021.
[9]. Siar, O., Benlatreche, Y., Dupuy, T., Dancette, S. and Fabrègue, D., Effect of severe welding conditions on liquid metal embrittlement of a 3rd-generation advanced high-strength steel. Metals, 10(9), p.1166. 2020.
[10]. Gáspár, M. and Balogh, A., GMAW experiments for advanced (Q+ T) high strength steels. Production Processes and Systems, 6(1), pp.9-24, 2013.
[11]. Enzinger, N., Cerjak, H., Böllinghaus+, T., Dorsch, T., Saarinen, K. and Roos, E., November. Properties of high strength steel s890 in dry and aqueous environments. In 1st. Int. Conf. Super-High Strength Steels. 2005.
[12]. Cerjak, H.H., Enzinger, N., Greiner, R. and Zenz, G., High Strength Steels for Hydropower Plants Design Concepts-Pressure Conduits. Verlag der Technischen Universität Graz. 2013.
[13]. Schröter, F. and Schütz, W., 2005. State of art in the production and use of high-strength heavy plates for hydropower applications. Proceedings of the High Strength Steel for Hydropower Plants, Graz, Austria, pp.5-6.
[14]. ***, www.esab.com, ESAB (Washington DC, USA)
[15].***, AG der Dillinger Hüttenwerke, Germania, https://en.dillinger.de/products/downloads/ (accesare la 18.10.2022).
[16]. ***, Thyssenkrupp AG, Germania, https://www.thyssenkrupp-steel.com/en/publications.html/ (accesare la 18.06.2022).
[17]. David et al. “Weldable high-strength steels: Challenges and engineering applications.” 2015.
[18]. ***, SR CEN ISO/TR 15608:2017 - Sudare. Ghid pentru un sistem de grupare a materialelor metalice
[19]. ***, SR EN 10025-3:2019 - Produse laminate la cald din oțeluri de construcții. Partea 3: Condiții tehnice de livrare pentru oțeluri de construcții sudabile cu granulație fină în stare normalizată/laminare normalizantă
[20]. ***, SR EN 10025-4+A1:2023 - Produse laminate la cald din oţeluri de construcţii. Partea 4: Condiţii tehnice de livrare pentru oţeluri de construcţii sudabile cu granulaţie fină obţinute prin laminare termomecanică

[21]. SR EN 10025-6+A1:2023 - Produse laminate la cald din oţeluri de construcţii. Partea 6: Condiţii tehnice de livrare pentru produse plate din oţeluri cu limită de curgere ridicată în stare călită şi revenită.
[22]. Lehnert, T. and Schröter, F., How Modern Steel Developments Can Help Optimizing Cost and Sustainability of Bridge Constructions. Dillinger Hütte. 2014.
[23]. Micloşi, V., Tratamente termice conexe sudării prin topire a oţelurilor Vol.I, Timişoara, Sudura, 2003 2 vol., ISBN 973-8359-10-4, Vol. 1 – Bibliogr. – ISBN 973-8359-11-2. 2003
[24]. Micloşi, V., Tratamente termice conexe sudării prin topire a oţelurilor Vol.II, Timişoara, Sudura, 2004 2 vol., ISBN 973-8359-10-4, Vol. 3 – Bibliogr. – ISBN 973-8359-12-0. 2004
[25]. Bodea, M., "Sudura si procedee conexe", Editura UTCLUJ, ISBN 978-606-737-143-7, 2016.
[26]. ***, https://www.totalmateria.com/en-us/articles/thermo-mechanical-control-process/ pdf (accesare la 12.11.2023).
[27]. Patel, J., Introduction to high strength structural steels, International Metallurgy Ltd. 2021.
[28]. I.Voiculescu, C.Rontescu, I.L.Dondea. Metalografia îmbinărilor sudate. Editura SUDURA, ISBN 978-973-8359-58-1, 2010
[29]. ***, www.schmitz-metallographie.de (accesare la 29.10.2023).
[30]. Lehto, P., Remes, H., Saukkonen, T., Hänninen, H. and Romanoff, J., Influence of grain size distribution on the Hall–Petch relationship of welded structural steel. Materials Science and Engineering: A, 592, pp.28-39.. ISSN, 2014.
[31]. Herion, S. and Scherf, S., High Strength Steels for Low Temperature Structural Applications. In Proc 8th Int Conf on Advances in Steel Structures. 2018.
[32]. ***, AAchen University, ISF - Welding and Joining Institute, 2005.
[33]. ***, SR EN 10149-2:2014 - Produse plate laminate la cald din oţeluri cu limită de curgere ridicată pentru deformare la rece. Partea 2: Condiţii tehnice de livrare pentru oţeluri obţinute prin laminare termomecanică
[34]. Mohrbacher, H., Metallurgical concepts for optimized processing and properties of carburizing steel. Advances in Manufacturing, 4(2), pp.105-114. 2016.
[35]. Mohrbacher, H., Property optimization in as-quenched martensitic steel by molybdenum and niobium alloying. Metals, 8(4), p.234. 2018.
[36]. ***, Voestalpine Grobblech GmbH, Linz, Austria, High strength and ultra high strength Thermomechanically Rolled fine-grained steels, Rolled fine-grained steels, Technical terms of delivery for heavy plates, Alform, 1 January, 2024.
[37]. ***, Lori Jo Vest |AHSS Guidelines Version 7.0, Jun 29, 2021, diponibila online la https://www.worldautosteel.org/, (accesare la 28.10.2023).
[38]. ***, SEW 088 : 2017 - Weldable non-alloy and low-alloy steels - recommendations for processing, in particular for fusion welding.
[39]. ***, SR EN 1011-1:2009 - Sudare. Recomandări pentru sudarea materialelor. Partea 1: Ghid general pentru sudarea cu arc electric
[40]. ***, SR EN 1011-2: 2002/A1:2004 - Sudare. Recomandări pentru sudarea materialelor metalice. Partea 2: Sudarea cu arc electric a oţelurilor feritice
[41]. Wongpanya, P., Boellinghaus, T., Lothongkum, G. and Kannengiesser, T., Effects of preheating and interpass temperature on stresses in S 1100 QL multi-pass butt-welds. Welding in the World, 52, pp.79-92. 2008.
[42]. Dehelean, D. Sudarea prin topire, Editura Sudura, Timişoara, ISBN 973-98049-1-8. 1997.
[43].***,Air Liquide Welding Cranes & Heavy Lifting Equipment, https://www.airliquide.com/sites/airliquide.com/files/th_cranes_and_heavy_lifting_w000370267_en.pdf (accesare la 28.10.2023).
[44]. S. Kou, Welding Metallurgy, 2nd Edition, John Wiley & Sons, Inc., New York, 2002.
[45]. Padhy, G.K. and Komizo, Y.I., Diffusible hydrogen in steel weldments: A status review. Transactions of JWRI, 42(1), pp.39-62. 2013.
[46]. Granjon, H., Cold cracking in the welding of steels. Indian Welding Journal, pp.43-53. 1973.

[47]. C.Rontescu, G. Iacobescu, D.T. Cicic, Sudarea prin topire, Vol. III, Editura Bren, ISBN 978-606-610-250-6, 2020.
[48]. Manivelmuralidaran, V., Sakthivel, M. and Balaji, M., Cold Crack Susceptibility studies on high strength low alloy steel 950A using tekken test. J Adv Chem, (3), pp.25-31. 2017.
[49]. Hong, K.A.N.G., Mingshan, F.A.N.G., Dongmei, J.I.A., Xueyi, F.U., Yurong, L.I.U., Lizhen, W.A.N.G. and Xiaofeng, Z.H.A.O., Effect of Heat input on Microstructure and Properties of Heat Affected Zone in 890 MPa Welded Tube for Crane Boom Service. STEEL PIPE, 53(2), pp.74-78. 2024.
[50]. Magudeeswaran, G., Balasubramanian, V. and Reddy, G.M., Hydrogen induced cold cracking studies on armour grade high strength, quenched and tempered steel weldments. International journal of hydrogen energy, 33(7), pp.1897-1908. 2008.
[51]. Gáspár, M., Effect of welding heat input on simulated HAZ areas in S960QL high strength steel. Metals, 9(11), p.1226. 2019.
[52]. ***, SR EN ISO 15614-1:2017/A1:2019 - Specificația și calificarea procedurilor de sudare pentru materiale metalice. Verificarea procedurii de sudare în vederea calificării. Partea 1: Sudarea cu arc electric și sudarea cu gaze a oțelurilor și sudarea cu arc electric a nichelului și a aliajelor de nichel. Amendament1.
[53]. Brezova, E., Masiar, H. and Radic, P., „Welding of high strength materials used in the manufacture special equipment". University Review, 8(3-4), pp.51-61. 2014.
[54]. C. Rontescu, G. Iacobescu, Sudarea prin topire, Vol. I, Editura Bren, Cod CNCSIS 96, ISBN 978-606-610-190-5, 2016.
[55]. Yang, D.X., Wang, X.H., Liu, Z.Y. and Sun, Y.F., Study on SH-CCT Diagram and Weldability of S890 Steel. Advanced Materials Research, 415, pp.865-868. 2012.
[56]. Peltonen, M., Weldability of high-strength steels using conventional welding methods, 2014.
[57]. Klein, M., Spindler, H., Luger, A., Rauch, R., Stiaszny P., and Eigelsberger, P. M., "Thermomechanically hot rolled high and ultra high strength steel grades-processing, properties and application., Materials Science Forum, 500-501, pp. 543-550. 2005.
[58]. Honeycomb, R. W. K., and Bhadeshia, H. K. D. H., Steels - microstructure and properties, Second Ed., London: Edward Arnold. 1995.
[59]. Mohrbacher, H., Principal effects of Mo in HSLA steels and cross effects with microalloying elements. Central Iron and Steel Research Institute (CISRI), pp.75-96. 2010.
[60]. Guillala, A., Abdelbakib, N., Gaceba, M. and Bettayeba, M., Effects of martensite-austenite constituents on mechanical properties of heat affected zone in high strength pipeline steels-review. Chem. Eng, 70, pp.583-588. 2018.
[61]. ***, ANTERA STEEL S.R.L. 2016, https://www.anterasteel.ro/ElementeAliere.aspx (accesare la 18.06.2022).
[62]. ***, Weld Magazine, https://sites.ualberta.ca/~ccwj/Assets/Teaching/MATE481/HRD_ Prediction_ of_Hardness/Supplemental_Material/hintze19_hardness_models_steel.pdf (accesare la 12.11.2023).
[63]. Górka, J., Janicki, D., Fidali, M. and Jamrozik, W., Thermographic assessment of the HAZ properties and structure of thermomechanically treated steel. International Journal of Thermophysics, 38, pp.1-21. 2017.
[64]. Węglowski, M.S. and Zeman, M., Prevention of cold cracking in ultra-high strength steel Weldox 1300. Archives of Civil and Mechanical engineering, 14(3), pp.417-424. 2014.
[65]. Dobosy, Á. and Lukács, J., The effect of the welding parameters on the properties of thermomechanically rolled high strength steels. In Proceedings of the MultiScience—XXX, microCAD International Multidisciplinary Scientific Conference, Miskolc, Hungary (pp. 21-22), ISBN 978-963-358-113-1, April 2016.
[66]. Cicic, D.T., Rontescu, C., Bogatu, A.M. and Petriceanu, C.S., August. Research regarding the influence of the preheating temperature on the welding dilution. In IOP Conference Series: Materials Science and Engineering (Vol. 400, No. 2, p. 022015). IOP Publishing. 2018.
[67].). Schaupp, T., Ernst, W., Spindler, H. and Kannengiesser, T., Hydrogen-assisted cracking of GMA welded 960 MPa grade high-strength steels. International journal of hydrogen energy, 45(38), pp.20080-20093. 2020.

[68]. ***, https://www.imoa.info/molybdenum-uses/molybdenum-grade-alloy-steels-irons/structural-steels-TMCP.php (accesare la 18.09.2022
[69]. Rontescu, C., Voiculescu, I., Iacobescu, G. and Cicic, D.T., Influence of the parameters preheating temperature and linear energy on the micrographic and macrographic characteristics of welded joints, UPB Sci. Bull., Series D, 71(2). 2009.
[70]. Celin, R., Berneti. J., Anica, D,. Balanti, S., Welding of the steel grade S890QL, Materials and technology, 48, pp. 931-935, ISSN 1580-2949. 2014.
[71]. Liu, X., Chung, K.F., Ho, H.C., Xiao, M., Hou, Z.X. and Nethercot, D.A., Mechanical behavior of high strength S690-QT steel welded sections with various heat input energy. Engineering Structures, 175, pp.245-256. 2018.
[72]. Bodea, M., December. New weldability model based on the welding parameters and hardness profile. In Powder Metallurgy and Advanced Materials. Materials Research Forum LLC (pp. 115-124). 2018.
[73]. Liu, T.Y., Qiu, X.B., Lu, Z.Y. and Dong, L.M., Estimation of cooling rate from 800 C to 500 C in the welding of intermediate thickness plates based on FEM simulation. Journal of Materials Science and Engineering B, 7(6), pp.258-267. 2017.
[74]. Kou, S., Welding metallurgy, New York: John Wiley & Sons, Inc. 1987.
[75]. American Welding Society, AWS,: Welding Hand Book, Miami: American Welding Society. 1981.
[76]. Terasaki, T. and Gooch, T. G., "Prediction of cooling time for ferrite-austenite. 1995.
[77]. Fiedler, M., Plozner, A., Rutzinger, B. and Scherleitner, W., Control of mechanical properties of high strength steels through optimized welding processes. Biul Inst Spawalnictwa, 5, pp.31-37. 2016.
[78]. Gyasi, E.A. and Kah, P., Structural integrity analysis of the usability of high strength steels (HSS). Reviews on Advanced Materials Science, 46(1). 2016.
[79]. Arora, A., Roy, G.G. and DebRoy, T., Cooling rate in 800 to 500 C range from dimensional analysis. Science and Technology of Welding and Joining, 15(5), pp.423-427. 2010.
[80]. Mičian, M., Frátrik, M., Trško, L., Gucwa, M., Winczek, J. and Skroński, Ł., Butt welding of thin sheets of S960MC steel. Welding Technology Review, 93. 2021.
[81]. ***, AWS A3.0M/A3.0:2020, An American National Standard, Standard Welding Terms and Definitions, Including Terms for Adhesive Bonding, Brazing, Soldering, Thermal Cutting, and Thermal Spraying,13th Edition. 2020.
[82]. ***, SR EN ISO 4063:2023 - Sudare, lipire tare, lipire moale și tăiere. Nomenclatorul procedeelor şi numere de referinţă
[83]. Coman, M.N., Rontescu, C., Bogatu, A.M., Cicic, D.T. and Florea, A., Industry 4.0 in welding processes in the automotive industry. Fiabilitate si Durabilitate - Fiability & Durability No 2/ 2023. Editura “Academica Brâncuşi” , Târgu Jiu, ISSN 1844 – 640X. 2023.
[84]. Coman, M.N., Rontescu, C., Bogatu, A.M., Cicic, D.T., Pîrvu, V., Implementation of robot welding in the context of Industry 4.0 development, Modtech 2023.
[85]. Ślęzak, T., Characteristics of MAG Welded Joints Made in Fine-Grained High-Strength Steel S960QL. Biuletyn Instytutu Spawalnictwa w Gliwicach, 62(6), pp.45-53. 2018.
[86]. Keränen, L., Pylvänäinen, M., Kaijalainen, A., Jokiaho, T., Tulonen, J., Hyvärinen, A., Vippola, M. and Kurvinen, E.,. Residual stresses of MAG-welded ultrahigh-strength steel rectangular hollow sections. Engineering Structures, 305, p.117719. 2024.
[87]. Mičian, M., Harmaniak, D., Nový, F., Winczek, J., Moravec, J. and Trško, L., Effect of the t 8/5 Cooling Time on the Properties of S960MC Steel in the HAZ of Welded Joints Evaluated by Thermal Physical Simulation. Metals, 10(2), p.229. 2020, 10, 229.
[88]. Ismar, H., Burzi, Z., Kapor, N.J. and Kokelj, T., Experimental Investigation of High-Strength Structural Steel Welds. Journal of Mechanical Engineering/Strojniški Vestnik, 58(6). 2012.
[89]. Lazic, V., Arsić, D., Aleksandrovic, S., Nikolic, R., Djordjevic, M. and Hadzima, B., Experimental investigations of the high-strength steel welded samples. 978-80-89296-21-7. 2017.

[90]. Mert, T., Gurol, U. and Tumer, M., The effect of heat input in multi-pass GMAW of S960QL UHSS based on weaving and stringer bead procedure on microstructure and mechanical properties of HAZ. Materials Research Express, 10(8), p.086507. 2023.
[91]. Mert, T., Gürol, U. and Tümer, M., The effect of weaving and non-weaving multi-pass procedure on microstructure and mechanical properties in GMAW of S960QL. The International Journal of Advanced Manufacturing Technology, 129(9), pp.4731-4742. 2023.
[92]. Liu, Z., Li, X., Pan, L., Gao, J. and Zhang, K., Effects of weld penetration modes on laser welding characteristics of a novel ultra-high strength steel for aerospace application. Journal of Manufacturing Processes, 90, pp.111-124. 2023.
[93]. Kahnamouei, J.T. and Moallem, M., Advancements in control systems and integration of artificial intelligence in welding robots: A review. Ocean Engineering, 312, p.119294. 2024.
[94]. Bayock, F.N., Kah, P., Mvola, B. and Layus, P., Experimental review of thermal analysis of dissimilar welds of High-Strength Steel. Reviews on Advanced Materials Science, 58(1), pp.38-49. 2019.
[95]. Chen, C., Chiew, S.P., Zhao, M.S., Lee, C.K. and Fung, T.C., Welding effect on tensile strength of grade S690Q steel butt joint. *Journal of Constructional Steel Research*, *153*, pp.153-168. 2019.
[96]. Chiew, S.P., Cheng, C., Zhao, M.S., Lee, C.K. and Fung, T.C., Experimental study of welding effect on S690Q high strength steel butt joints. *ce/papers*, *3*(3-4), pp.701-706. 2019.
[97]. Rontescu, C., Cicic, D.T., Iacobescu, G. and Amza, G.C., The influence of the welding current polarity on the geometric configuration of the bead. Advanced Materials Research, 1088, pp.797-801. 2015.
[98]. Rontescu, C., Iacobescu, G., Sudarea prin topire, Vol.II, Editura Bren, ISBN 978-606-610-225-4, 2019.
[99]. Tarn T.J. et al., Robotic Welding, Intelligence and Automation, LNEE, 88, pp. 369-374, 2011.
[100]. Muñoz, M.Á.Z., Escoto, P.A.O. and Gordillo, G.B., June. Automated MIG Welding Application: An Industrial Case Study. In International Conference on Machine and Industrial Design in Mechanical Engineering (pp. 627-635). Cham: Springer International Publishing. 2021.
[101]. Kah, P. and Martikainen, J., Current trends in welding processes and materials: improve in effectiveness. Rev. adv. mater. Sci, 30(2), pp.189-200. 2012.
[102]. Voiculescu, I., Geanta, V., Rusu, C.C., Mircea, O., Mistodie, L.R. and Scutelnicu, E., Research on the Metallurgical Behaviour of X70 Steel subjected to Multi-Wire Submerged Arc Welding. Annals of "Dunarea de Jos" University of Galati. Fascicle XII, Welding Equipment and Technology, 27, pp.38-46. 2016.
[103]. Scutelnicu, E., Rusu, C.C., Georgescu, B., Mircea, O. and Bormambet, M., Mechanical behaviour of welded joints achieved by multi-wire submerged arc welding. Advanced Materials Research, 1143, pp.52-57. 2017.
[104]. Puchianu, M., **Florea, A.,** Solomon, G., Duma, I. and Pascu, G., studies regarding submerged arc welding of duplex stainless steel in shipbuilding industry. U.P.B. Sci. Bull., Series D, Vol. 85, Iss. 3, ISSN 1454-2358. 2023.
[105]. Kah, P., Layus, P. and Ndiwe, B., Submerged arc welding process peculiarities in application for Arctic structures. *AIMS Materials Science*, *9*(3), pp.498-511. 2021.
[106]. Layus, P., Usability of the submerged arc welding (SAW) process for thick high strength steel plates for Arctic shipbuilding applications. 2017.
[107]. Layus P, Kah P, Gezha V. Advanced submerged arc welding processes for Arctic structures and ice-going vessels. Proceedings of the Institution of Mechanical Engineers, Part B: Journal of Engineering Manufacture. 2018.
[108]. Layus, P., Kah, P., Kesse, M. and Gyasi, E., June. Submerged Arc Welding Process Productivity in Welding Thick High Strength Steel Plates Used for Arctic Applications. In *ISOPE International Ocean and Polar Engineering Conference* (pp. ISOPE-I). ISOPE. 2017.
[109]. Cicic, D.T., Rontescu, C., Amza, C.G. and Chivu, O.R., The combined effect of chemical elements on the properties of a layer deposited by welding. Rev. Chim.(Bucharest), 66(9), pp.1299-1301. 2015.

[110]. Sahoo, A. and Tripathy, S., Development in plasma arc welding process: a review. Materials Today: Proceedings, 41, pp.363-368. 2021.
[111]. Wu, C.S., Wang, L., Ren, W.J. and Zhang, X.Y., Plasma arc welding: Process, sensing, control and modeling. Journal of manufacturing processes, 16(1), pp.74-85. 2014.
[112]. Tashiro, S., Interaction mechanism of arc, keyhole, and weld pool in keyhole plasma arc welding: a review. Materials, 17(6), p.1348. 2024.
[113]. ***,Ionix Oy, Finlanda, https://www.ionix.fi/en/technologies/laser-processing/hybrid-laser-welding/ (accesare la 28.10.2023).
[114]. ***,CLOOS GmbH, Germania, https://www.cloos.de/de-en/processes/details/laser-hybrid-weld/ (accesare la 28.10.2023).
[115]. ***,Fronius International GmbH, Austria, https://www.fronius.com/en/welding-technology/products/robotic-welding/migmag-high-performance/laserhybrid/laserhybrid (accesare la 28.10.2023).
[116]. Lahdo, R., Seffer, O., Springer, A., Kaierle, S. and Overmeyer, L., GMA-laser hybrid welding of high-strength fine-grain structural steel with an inductive preheating. Physics Procedia, 56, pp.637-645. 2014.
[117]. Sisodia, R.P.S. and Gáspár, M., An approach to assessing S960QL steel welded joints using EBW and GMAW. Metals, 12(4), p.678. 2022.
[118]. Tümer, M., Domitner, J. and Enzinger, N., Electron beam and metal active gas welding of ultra-high-strength steel S1100MC: influence of heat input. The International Journal of Advanced Manufacturing Technology, pp.1-12. 2022.
[119]. Błacha, S., Węglowski, M.S., Dymek, S. and Kopyściański, M., Microstructural and mechanical characterization of electron beam welded joints of high strength S960QL and Weldox 1300 steel grades. Archives of Metallurgy and Materials, 62. 2017
[120]. ***, SR EN ISO 17637:2017 - Examinări nedistructive ale sudurilor. Examinarea vizuală a îmbinărilor sudate prin topire
[121]. ***, SR EN ISO 23277:2015 - Examinări nedistructive ale sudurilor. Examinarea cu lichide penetrante a sudurilor. Niveluri de acceptare
[122]. ***, SR EN ISO 3452-1:2021 - Examinări nedistructive. Examinare cu lichide penetrante. Partea 1: Principii generale
[123]. ***, SR EN ISO 3452-4:2002 - Examinări nedistructive. Examinări cu lichide penetrante. Partea 4: Echipament
[124]. ***, SR EN ISO 5817:2023 - Sudare. Îmbinări sudate prin topire din oţel, nichel, titan şi aliajele acestora (cu excepţia sudării cu fascicule de energie). Niveluri de calitate pentru imperfecţiuni.
[125]. ***, SR EN ISO 17640:2019 - Examinări nedistructive ale îmbinărilor sudate. Examinare cu ultrasunete. Tehnici, niveluri de examinare și evaluare
[126]. ***, https://www.tcontrol.ro/ultrasunete/UTTransducers/. (accesare la 18.06.2021).
[127]. ***, SR EN 10027-1:2017 - Sisteme de simbolizare a oţelurilor.Partea 1: Simbolizarea alfanumerică.
[128]. ***, Certificatul de calitate al materialului de bază. (Atașat la Anexa 1).
[129]. Zgură, Gh., Iacobescu G., Rontescu C., Cicic D.T. - Tehnologia sudării prin topire, Editura Politehnica Press , Bucureşti, 2007.
[130]. ***, SR EN 10204:2005 - Produse metalice. Tipuri de documente de inspecţie
[131]. Gorni, A.A., Steel forming and heat treating handbook. São Vicente, Brazil, 24. 2011.
[132]. ***, SR EN ISO 16834:2012 - Materiale consumabile pentru sudare. Sârme electrod, sârme vergele şi depuneri prin sudare pentru sudarea cu arc electric în mediu de gaz protector a oţelurilor cu limită de curgere ridicată. Clasificare
[133]. ***, Certificatul de calitate al materialului de adaos. (Atașat la Anexa 2).
[134]. ***, Dillinger Hütte GTS: Dillimax Technical Information No. III/2007, p. 25.
[135]. ***, SR EN ISO 15613:2004 - Specificaţia şi calificarea procedurilor de sudare pentru materiale metalice. Calificarea bazată pe o încercare de sudare înainte de fabricaţie

[136]. **Florea, A.,** Rontescu, C., Bogatu, A.M., Cicic, D.T., Coman M.N., Research regarding the measurement possibilities of the thermal cycle in welding, Fiabilitate si Durabilitate - Fiability & Durability No 2/ 2023. Editura "Academica Brâncuşi" , Târgu Jiu, ISSN 1844 – 640X. 2023.
[137]. Gh. Solomon, D.T. Cicic, Teotia proceselor de sudare Vol.I, Vol.II, Editura Bren, 2010.2301-2318, Bariloche, 2004
[138]. Micloşi, V., Bazele proceselor de sudare, EDP, București, 1982.
[139]. SR EN ISO 9692-1:2014 - Sudare şi procedee conexe. Tipuri de pregătire a îmbinării. Partea 1: Sudare manuală cu arc electric cu electrod învelit, sudare cu arc electric cu electrod fuzibil în mediu de gaz protector, sudare cu gaze, sudare WIG şi sudare cu fascicule de energie a oţelurilor.
[140]. ***, SR EN ISO 14175:2008 - Materiale consumabile pentru sudare. Gaze şi amestecuri de gaze pentru sudarea prin topire şi procedee conexe.
[141]. Unnikrishnakurup, S., Krishnamurthy, C.V. and Balasubramaniam, K., Monitoring TIG welding using infrared thermography–simulations and experiments. Przegląd Elektrotechniczny, 92, pp.1-18. 2016.
[142]. Rontescu, C., Voiculescu, I., Iacobescu, G., Dumitrascu, C. and Cicic, D.T., Analysis of the thermal field for TIG welding by using infrared thermography. UPB Scientific Bulletin, Series D: Mechanical Engineering, 70(3), pp.55-60. 2008.
[143]. Stăncioiu, A., Releasing the welded parts through thermal treatments, Fiabilitate si Durabilitate - Fiability & Durability No 1/ 2023.
[144]. Bermejo, V.M.A., Hurtig, K., Hosseini, V.A., Karlsson, L. and Svensson, L.E., October. Monitoring thermal cycles in multi-pass welding. In *Proceedings of the 7th International Swedish Production Symposium (SPS-16), Lund, Sweden* (pp. 25-27). 2016.
[145]. X.F Liu, C.B. Jia, C.S. Wua, G.K. Zhang; J.Q Gao, Measurement of the keyhole entrance and topside weld pool geometries in keyhole plasma arc welding with dual CCD cameras, J. Mater. Process. Technol. 248, 2017, pp.39-48.
[146]. Pinto-Lopera J.E., J.M.S.T. Motta, S.C.A. Alfaro, Real-Time Measurement of Width and Height of Weld Beads in GMAW Processes, Sensors 2016, 16, pp.1-14.
[147]. B. Silwal, M. E, Santangelo, Effect of vibration and hot-wire gas tungsten arc (GTA) on the geometric shape, J. Mater. Process. Technol., 251, pp. 138-145. 2018.
[148]. Lahtinen, T., Vilaça, P., Peura, P., Mehtonen, S. MAG Welding Tests of Modern High Strength Steels with Minimum Yield Strength of 700 MPa. Appl. Sci. 2019.
[149]. **Florea, A.,** Petriceanu, S.C., Rontescu, C., Bogatu, A.M., Cicic, D.T., Thermal field measurement during welding using infrared thermography, University Politehnica of Bucharest Scientific bulletin series B-chemistry and materials science, Volume85, Issue3, Page167-178, 2023.
[150]. ***, SR EN ISO 6520-1:2007 - Sudare şi procedee conexe. Clasificarea imperfecţiunilor geometrice din îmbinările sudate ale materialelor metalice. Partea 1: Sudare prin topire.
[151]. ***, SR EN ISO 17635:2017 - Examinări nedistructive ale sudurilor. Reguli generale pentru materiale metalice.
[152]. ***, SR EN ISO 9712:2022 - Examinări nedistructive. Calificarea și certificarea personalului pentru examinări nedistructive
[153]. ***, SR EN ISO 3059:2013 - Examinări nedistructive. Examinarea cu lichide penetrante şi cu pulberi magnetice. Condiţii de observare
[154]. ***, SR EN ISO 11666:2018 - Examinări nedistructive ale sudurilor. Examinare cu ultrasunete. Niveluri de acceptare
[155]. **Florea, A.,** Rontescu, C., Bogatu, A.M., Cicic, D.T., Assessment of the hardness of S890QL material welded joins. 2024.
[156]. ***, SR EN ISO 6507-1:2023 - Materiale metalice. Încercarea de duritate Vickers. Partea 1: Metodă de încercare
[157]. ***, SR EN ISO 9015-1:2011 - Încercări distructive ale îmbinărilor sudate din materiale metalice. Încercarea de duritate. Partea 1: Încercarea de duritate a îmbinărilor sudate cu arc electric

[158]. ***, SR EN ISO 9015-2:2016 - Încercări distructive ale îmbinărilor sudate din materiale metalice. Încercarea de duritate. Partea 2: Încercarea de microduritate a îmbinărilor sudate
[159]. Python Software Foundation, 2024. Python 3.12. Disponibil la: https://www.python.org (Accesat 17.10.2024).
[160]. Plotly, 2024. Plotly Library. Disponibil la: https://plotly.com/python/ (Accesat 17.10.2024).
[161]. ***, SR EN ISO 4136:2022 - Încercări distructive ale sudurilor din materiale metalice. Încercarea la tracţiune transversală
[162]. ***, SR EN ISO 6892-1:2020 - Materiale metalice – Încercarea la tracțiune – Partea 1: Metodă de încercare la temperatura ambiantă
[163]. ***, SR EN ISO 148-1:2017 - Materiale metalice. Încercarea de încovoiere prin şoc pe epruveta Charpy. Partea 1: Metodă de încercare
[164]. ***, SR EN ISO 9016:2022 - Încercări distructive ale îmbinărilor sudate din materiale metalice. Încercare la încovoiere prin şoc. Poziţie a epruvetei, orientare a crestăturii şi examinare
[165]. ***, SR EN ISO 17639:2022 - Încercări distructive ale îmbinărilor sudate din materiale metalice. Examinarea macroscopică şi microscopică a îmbinărilor sudate
[166]. ***, SR EN ISO 643:2020 - Oțeluri. Determinarea micrografică a mărimii aparente a grăuntelui
[167]. Florin BODE, Simularea numerică a proceselor de transfer termic, UTPRESS Cluj-Napoca, 2021
[168]. ***, Simcenter 3D – Capabilități extinse de editare a geometriei și simulare, https://www.digitaltwin.ro/produse-siemens-plm/simcenter-3d/ (accesare la 18.06.2021).